2016-06

Comparison of two railgun power supply architectures to quantify the energy dissipated after the projectile leaves the railgun

Stewart, Mitchell C.

Monterey, California: Naval Postgraduate School

NAVAL POSTGRADUATE SCHOOL

MONTEREY, CALIFORNIA

THESIS

COMPARISON OF TWO RAILGUN POWER SUPPLY ARCHITECTURES TO QUANTIFY THE ENERGY DISSIPATED AFTER THE PROJECTILE LEAVES THE RAILGUN

by

Mitchell C. Stewart

June 2016

Thesis Advisor: Alexander L. Julian
Co-Advisor: Giovanna Oriti

THIS PAGE INTENTIONALLY LEFT BLANK

REPORT DOCUMENTATION PAGE			*Form Approved OMB No. 0704–0188*
Public reporting burden for this collection of information is estimated to average 1 hour per response, including the time for reviewing instruction, searching existing data sources, gathering and maintaining the data needed, and completing and reviewing the collection of information. Send comments regarding this burden estimate or any other aspect of this collection of information, including suggestions for reducing this burden, to Washington headquarters Services, Directorate for Information Operations and Reports, 1215 Jefferson Davis Highway, Suite 1204, Arlington, VA 22202-4302, and to the Office of Management and Budget, Paperwork Reduction Project (0704-0188) Washington, DC 20503.			
1. AGENCY USE ONLY ***(Leave blank)***	**2. REPORT DATE** June 2016	**3. REPORT TYPE AND DATES COVERED** Master's thesis	
4. TITLE AND SUBTITLE COMPARISON OF TWO RAILGUN POWER SUPPLY ARCHITECTURES TO QUANTIFY THE ENERGY DISSIPATED AFTER THE PROJECTILE LEAVES THE RAILGUN			**5. FUNDING NUMBERS**
6. AUTHOR(S) Mitchell C. Stewart			
7. PERFORMING ORGANIZATION NAME(S) AND ADDRESS(ES) Naval Postgraduate School Monterey, CA 93943-5000			**8. PERFORMING ORGANIZATION REPORT NUMBER**
9. SPONSORING /MONITORING AGENCY NAME(S) AND ADDRESS(ES) N/A			**10. SPONSORING / MONITORING AGENCY REPORT NUMBER**
11. SUPPLEMENTARY NOTES The views expressed in this thesis are those of the author and do not reflect the official policy or position of the Department of Defense or the U.S. Government. IRB Protocol number ____N/A____.			
12a. DISTRIBUTION / AVAILABILITY STATEMENT Approved for public release; distribution is unlimited			**12b. DISTRIBUTION CODE**

13. ABSTRACT (maximum 200 words)

Railgun muzzle flash, or post-fire arcing, is a major concern to the Navy because of the potential associated thermal stresses. In this thesis, we compared two railgun power supplies in Matlab Simulink to quantify their associated post-fire energy. When the armature exits the rails, a finite energy from the railgun pulsed-power supply is inductively stored in the rails and discharges at the muzzle. This energy, which is due to the loss of the low-voltage electrical contact that is ordinarily between the armature and the rail, is forced by the system inductance to flow as an electrical discharge, creating a muzzle flash. Quantification of this post-fire rail energy in our simulation from both the existing railgun power supply and the proposed power supply—a thyristor-based power supply versus a buck-boost converter, respectively—reveals that the buck-boost converter topology is better suited for the railgun, particularly at minimizing the post-fire muzzle energy. The minimization of the post-fire energy allows for an extended rail life and potentially longer usage.

14. SUBJECT TERMS railgun, power supply, post-fire energy			**15. NUMBER OF PAGES** 79
			16. PRICE CODE
17. SECURITY CLASSIFICATION OF REPORT Unclassified	**18. SECURITY CLASSIFICATION OF THIS PAGE** Unclassified	**19. SECURITY CLASSIFICATION OF ABSTRACT** Unclassified	**20. LIMITATION OF ABSTRACT** UU

NSN 7540–01-280-5500 Standard Form 298 (Rev. 2–89)
Prescribed by ANSI Std. 239–18

THIS PAGE INTENTIONALLY LEFT BLANK

Approved for public release; distribution is unlimited

COMPARISON OF TWO RAILGUN POWER SUPPLY ARCHITECTURES TO QUANTIFY THE ENERGY DISSIPATED AFTER THE PROJECTILE LEAVES THE RAILGUN

Mitchell C. Stewart
Lieutenant, United States Navy
B.S., Johnson & Wales University, 2009

Submitted in partial fulfillment of the
requirements for the degree of

MASTER OF SCIENCE IN ELECTRICAL ENGINEERING

from the

NAVAL POSTGRADUATE SCHOOL
June 2016

Approved by: Alexander L. Julian
Thesis Advisor

Giovanna Oriti
Co-Advisor

R. Clark Robertson
Chair, Department of Electrical and Computer Engineering

THIS PAGE INTENTIONALLY LEFT BLANK

ABSTRACT

Railgun muzzle flash, or post-fire arcing, is a major concern to the Navy because of the potential associated thermal stresses. In this thesis, we compared two railgun power supplies in Matlab Simulink to quantify their associated post-fire energy. When the armature exits the rails, a finite energy from the railgun pulsed-power supply is inductively stored in the rails and discharges at the muzzle. This energy, which is due to the loss of the low-voltage electrical contact that is ordinarily between the armature and the rail, is forced by the system inductance to flow as an electrical discharge, creating a muzzle flash. Quantification of this post-fire rail energy in our simulation from both the existing railgun power supply and the proposed power supply—a thyristor-based power supply versus a buck-boost converter, respectively—reveals that the buck-boost converter topology is better suited for the railgun, particularly at minimizing the post-fire muzzle energy. The minimization of the post-fire energy allows for an extended rail life and potentially longer usage.

THIS PAGE INTENTIONALLY LEFT BLANK

TABLE OF CONTENTS

THIS PAGE INTENTIONALLY LEFT BLANK

LIST OF FIGURES

LIST OF TABLES

THIS PAGE INTENTIONALLY LEFT BLANK

LIST OF ACRONYMS AND ABBREVIATIONS

BEMF	Back electromagnetic force
EM	Electromagnetic
EMF	Electromagnetic Force
I-V	Current Voltage
LRC	Inductor Resistor Capacitor
PFN	Pulse Forming Network
RC	Resistor Capacitor

THIS PAGE INTENTIONALLY LEFT BLANK

ACKNOWLEDGMENTS

I would like to give many thanks to Dr. Alexander Julian for his unwavering support and guidance throughout the completion of my thesis. Your time and dedication to my research and your ability to help me focus on the underlying objective of my thesis is greatly appreciated. The lessons I have learned throughout this research will benefit me throughout my career. It was a pleasure and privilege sitting through your classes, and conducting research with you. Thank you.

THIS PAGE INTENTIONALLY LEFT BLANK

I. INTRODUCTION

The ability to conduct long-range fire support while keeping away from the coastal defenses of a potential adversary is an attractive prospect to the Department of the Navy. The application of railgun technology is a military weapon that makes this possible for the Navy. The Navy initiated the development of the electromagnetic (EM) railgun as a long-range weapon system designed to fire projectiles at very long ranges with enormous velocities, up to Mach 7. In contrast to current weapon systems, which use chemical propellants to launch projectiles, the EM railgun uses large electrical currents to generate strong magnetic fields which accelerate projectiles (armature) to speeds of over seven times the speed of sound (2400 m/s) [1]. Given such an enormous velocity, the projectile with a given mass can deliver impressive kinetic energy that is equivalent to a 5-inch gun on impact [1]. The potential of the EM railgun renders the need to store dangerous explosives associated with the conventional warheads unnecessary. The EM Railgun gives the U.S. Navy a major advantage in many mission areas. With the extended range of the EM railgun, the U.S. Navy is capable of effectively conducting numerous warfare requirements, such as long-range strikes at sea or land, ship defense, and precise long-range naval fire support.

A. OBJECTIVE

The objective of this research is to compare the state-of-the-art power supply power for a railgun, which is a thyristor-based power supply, as presented in [2] and [3], to a buck-boost converter-based power supply. Comparison of each of the power supplies is conducted by simulating the voltage and current stresses of each supply in order to quantify the post-fire energy stored within the rails after the projectile leaves the gun. The simulation will outline some critical performance characteristics of a buck-boost power supply as compared to a thyristor-based power supply. Some of the critical performance characteristics examined in the simulation are:

- The buck-boost and thyristor current waveform shapes
- Load-current shaping for both power supplies

- Post-firing energy comparison from both power supplies after the shot
- Armature velocity due to energy transference

B. RAILGUN THEORY

A simple equivalent circuit is illustrated in Figure 1 and represents an electromagnetic model of a railgun. In the illustration, a central free moving mass *m* is between two conducting rails a spacing *W* apart. The magnetic field intensity $\vec{H}$ generated by the current *I* through the rails is a function of the distance *W* from the center of the rail.

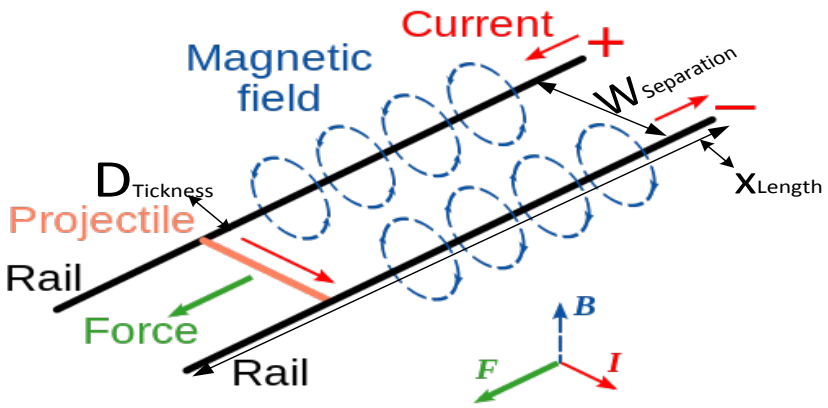

Figure 1. Railgun Model. Adapted from [4].

The magnetic field intensity $\vec{H}$ is calculated from

$$\int \vec{H} \cdot d\vec{l} = H 2\pi W = i \Rightarrow H(W) = \frac{i}{2\pi W} \tag{1}$$

where $\vec{H}$ is the magnetic field intensity, $\vec{l}$ is the length of the rails, *W* is the spacing between the rails and *i* is the current [2]. The magnetic flux Φ_m around the top rail is calculated by taking the integral of the dot product of the magnetic field $\vec{B}$ and the surface $\vec{S}$, that is, the area between the rails and from the projectile position along the length of the gun *x* [5]:

$$\Phi_m = \int \vec{B} \cdot d\vec{S} = x \frac{\mu_o}{2\pi} \int_{w_2}^{w_1} \frac{1}{W} dw = L' x \frac{i}{2}. \quad (2)$$

The coefficient μ_o is the permeability of free space, and the coefficient L' is the "inductance gradient" of the rails and is dependent on the geometry of the rails. The inductance gradient is

$$L' = (\mu_o / \pi) \ln(1 + W / D) \quad (3)$$

where D is the thickness of each rail [5].

The effect of friction on the projectile can be very small. Friction from air in the rails is also very small. Friction from the projectile touching the rails may, however, be significant depending on the construction of the rails [5]. Neglecting friction, the electromagnetic force F acting on the mass m is

$$F = (\mu_o I^2 / 2\pi) \ln(1 + W / D) = L' I^2 / 2, \quad (4)$$

where I is the current in the rails. From (4), we can calculate the velocity and acceleration of the mass in the railgun, assuming an ideal railgun model, where the current I is constant. The acceleration of the armature is determined by the product of the inductance gradient L' and the current I squared divided by twice the mass of the armature,

$$\frac{dv}{dt} = L' I^2 / 2m. \quad (5)$$

From the integrand of the acceleration,

$$\int dv = \left(L' I^2 / 2m \right) \int dt \quad (6)$$

we get the velocity v of the armature,

$$v = (L^{'} I / 2m)Q\,, \tag{7}$$

where Q is the charge delivered by the current I. The displacement, or the distance the projectile traveled through the rails, is

$$x = \left(L^{'} / 2m\right)\left(\int_0^Q qdq\right) = L^{'}Q^2 / 4m = \left(m / L^{'}\right)\left(v / I\right)^2. \tag{8}$$

From (8), we can rewrite the velocity v in term of x [5],

$$v = I\left(L^{'}x / m\right)^{1/2}. \tag{9}$$

The time t needed for the projectile to travel a distance x can be calculated from

$$t_f = Q / I \Rightarrow (2 / I)(mx / L^{'})^{1/2}, \tag{10}$$

as defined in [5].

In any railgun design, as described in Maier [5], some critical parameters must be considered to attain a desired velocity for a given projectile mass. The projectile velocity depends upon its mass, the inductance gradient, which is a function of the rails' separation, the length of time the current must be maintained, and the magnitude of the current. These interdependent relationships are critical in designing an appropriate power system [5]. In an ideal railgun model, given a constant current, as the projectile accelerates, magnetic flux Φ builds up in the space behind the moving projectile. Based on Faraday's law, which describes the interaction between an electric circuit and a magnetic field creating a magnetic force, the voltage V needed to hold the current constant must increase as the projectile gathers speed [5]:

$$V = d\Phi / dt = d(L^{'}xI) / dt = L^{'}Idx / dt\,. \tag{11}$$

Substituting (9) into (11), we get

$$V = L^{'}I\left(I\left(L^{'}x / m\right)^{1/2}\right) = I^2(L^{'})^{3/2}\left(x / m\right)^{1/2} \tag{12}$$

In (11) and (12), the voltage is the time derivative of the magnetic flux, which changes as the projectile travels through the rails. This voltage is related to the inductance gradient L', the rail length x and current I [5]. The instantaneous power P can be calculated from the product of the voltage and the current using [5]

$$P = I^2 (L')^{3/2} (x/m)^{1/2} I \,. \tag{13}$$

From (13), the power P increases as the voltage holding the current constant increases. Because the voltage changes as the projectile travels through the rails, the power which is also a function of the voltage and current, increases with the square root of the distance the projectile travels down the rails [5]. Equations (1) through (13) are representative of a general description of an ideal railgun model, such as one depicted in Figure 1 and Maier [5].

THIS PAGE INTENTIONALLY LEFT BLANK

II. POWER SUPPLY MODELING

Our objective in this chapter is to present the modeling of the buck-boost and thyristor Pulse Forming Networks (PFN). The illustrative equations outlined in [5] provide a framework from which the appropriate railgun pulse power models can be created. Using Simulink, we compared and quantified the railgun post-fire energy, evaluated component stresses and determined the efficiency at which energy was delivered to the rail from each prospective power supply.

The present railgun power supply architecture is a thyristor-based capacitor discharge power supply. This thyristor-based power supply is replaceable with a buck-boost power supply. The buck-boost power supply shows promise in minimizing muzzle energy and, potentially, has greater efficiency in delivering energy to the rails. The advantage of the buck-boost circuit is primarily due to the ability to control the current of the circuit. By controlling the current to the rails, the post-fire transient energy, which typically dissipates in the rail as heat from arcing, can be diminished. The diminished post-fire energy allows for an extended life of the rails.

A. THYRISTOR MODEL

Using Simulink, we modeled three thyristor-based capacitor discharge power supplies connected in parallel. Each is similar to the model shown in Figure 2. In our model, we simulated and quantified some critical performance characteristics of the thyristor power supply, mainly the shaping of the current to the load and transient current characteristics. The model has three block sets labeled thyristor_1, thyristor_2 and thyrisor_3. Within each block set lay the equivalent circuits shown in Figure 2, with initial inputs sent through an adder, multiplied by a $1/L$ gain, and then sent to an integrator labeled thyristor current. This integrator calculates the output thyristor current. This output current is negated, sent through a gain ($1/C$) and then integrated, generating the capacitor voltage. The thyristor current is negatively fed back through a 1-mΩ resistor to model the voltage drop across the inductor resistance (Gain_3 in Figure 2). The gating of each thyristor is interleaved such that they are gated one after the other in order to

interleave the pulses. Another measure typically utilized to reduce turn-on stress for this circuit when series connected thyristors are used is to place a resistor and a resistor-capacitor (RC) snubber in parallel with each thyristor. This mitigates imbalanced voltage during turn-on events. An equivalent thyristor circuit is shown in Figure 3.

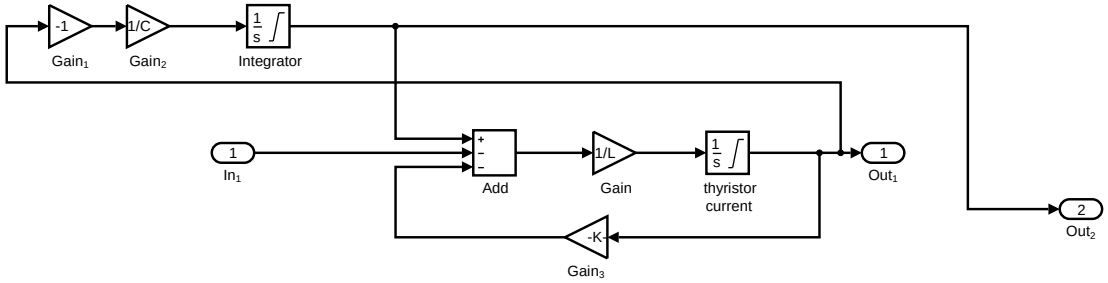

Figure 2. Simulink Model of a Single Thyristor Circuit.

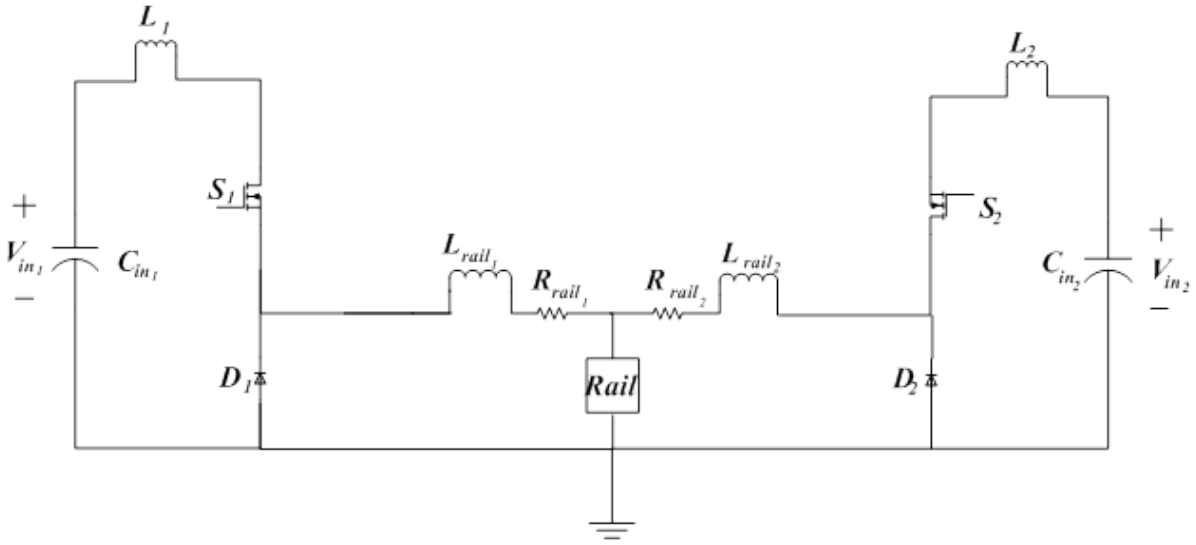

Figure 3. Thyristor Circuit. Adapted from [2].

The equivalent thyristor circuit illustrated in Figure 4 shows the commutation of the capacitor current to the diode. On the right side of Figure 4, a feedback diode placed between the thyristor and the capacitor ground is necessary to prevent reverse voltage on the capacitor. The commutation moment, when for a short interval both the diode and the

thyristor are conducting, is depicted in the left side of Figure 4. The simulations studied in this thesis treat this commutation event as an ideal, instantaneous action.

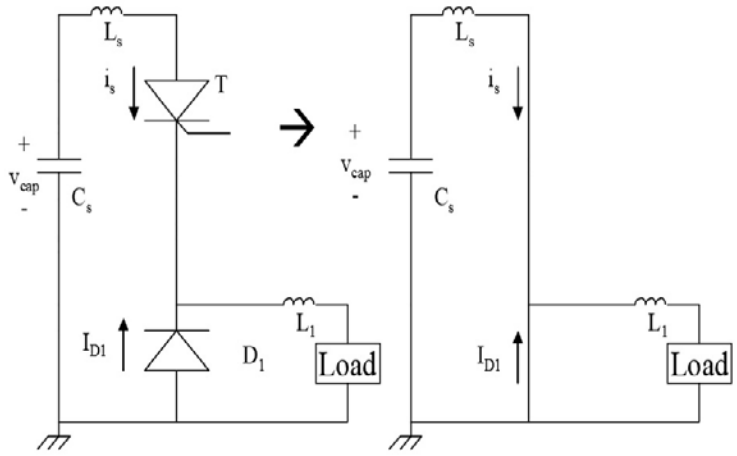

Figure 4. Equivalent Circuit during Commutation. Adapted from [2].

When the thyristor switch S_1 in Figure 3 is closed, the circuit can be modeled as an Inductor Resistor Capacitor (LRC) circuit but will have a non-oscillatory behavior since the current in the thyristor is not able to reverse. The characteristic of the current and voltage is determined from [5]

$$L_{rail} d^2q / dt^2 + R_{rail} dq / dt + q / c = 0 . \quad (14)$$

The current through the inductor becomes

$$I_L = dq / dt \quad (15)$$

where q is the charge. At the initial condition, the charge $q(0)$ on the capacitor is

$$q(0) = cV_o \quad (16)$$

where V_0 is the initial capacitor voltage. An illustration of the capacitor voltage after $t = 0$ is illustrated in Figure 5, when the switch S_1 closes as the capacitor discharges over a period of about 2 ms [2].

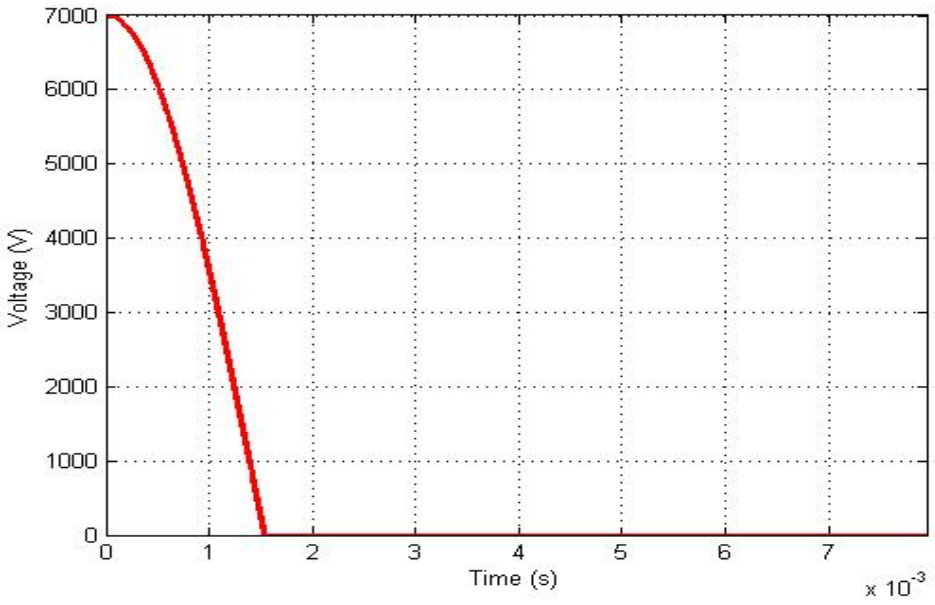

Figure 5. Capacitor Voltage across the Thyristor.

The inductor current is illustrated in Figure 6.

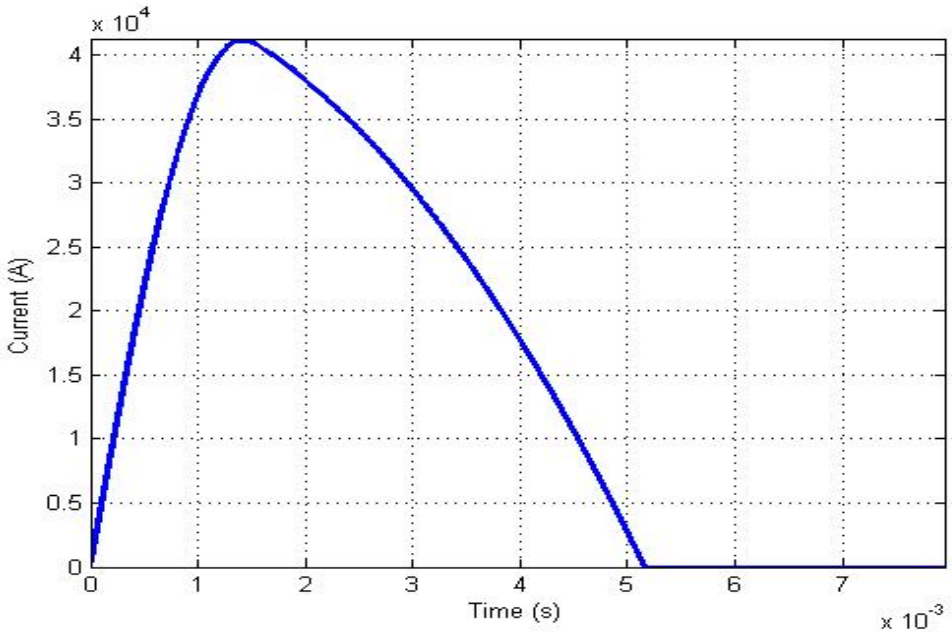

Figure 6. Thyristor Current over a 6.0-ms Time Period.

The current through the inductor is a maximum at time $t = 1$. The period and the angular frequency ω are related by

$$\tau = \frac{2\pi}{\omega}. \tag{17}$$

Parameters used in the calculation of the power supply are based on the values listed in Table 1.

Table 1. Parameters Used in Design of Simulated Railgun in the Model.

Variable	Description	Value	Units
L'	Inductance gradient of the rail	5×10^{-7}	H/m
$\mathbf{L_{rail}}$	Inductance due to transient	2×10^{-6}	H
m	Armature/projectile mass	3.125	kg
Rail	Length of the conductors	10	m
$\mathbf{R_{prime}}$	Resistance gradient of the rail	6×10^{-5}	Ω/m
$\mathbf{R_{20}}$	Rail and cable initial resistance	6×10^{-5}	Ω
$\mathbf{R_{rail}}$	Rails resistance	30×10^{-3}	Ω
C	Input capacitor	6×10^{-3}	F
$\mathbf{C_2}$	Second thyriator input Capacitor	9×10^{-3}	F

Upon completing the thyristor power supply model, we constructed the buck-boost power supply model. The buck-boost power supply modeled in Simulink allowed us to compare the efficiency of both power supplies ability to deliver energy to the rails and to analyze the post-fire transient in the rails.

B. BUCK-BOOST CONVERTER MODEL

Our objective in the following discussion is to outline the construction and operation of the buck-boost circuit. The modeling of this buck-boost converter was based on the schematic illustrated in Figure 7. In our Simulink model, we constructed the circuit using equation blocks to calculate and simulate voltages and currents in each component. Each switch in the schematic was modeled in Simulink using ideal switch models.

The energy delivered to the rail from the buck-boost converter is determined by control signals from two proportional-integral (PI) controllers. The control signals determine the appropriate duty cycle for the two main switches in the circuit, S_1 and S_2. If S_1 is conducting, the voltage drop across the inductor is the capacitor voltage minus the drop of the inductor resistance. This voltage drop is subtracted from the capacitor input voltage; this calculation is illustrated in Figure 8. This voltage drop is represented with a content block that has a value of 1mΩ in the model. The inductor current is represented in Figure 8, where the difference in the input capacitor voltage and the resistance voltage drop times the reciprocal of the inductor is integrated to generate the inductor current.

When S_2 is gated, the second buck-boost circuit behaves similarly to the first, as explained previously. The ability to control the current in the buck-boosts circuit is critical in minimizing the post-fire transient in the rails. By stopping the conduction of current to the rail at the point where the projectile exits the gun, we minimize the transient energy and prevent the input capacitor from fully discharging in an arc, thereby retaining a greater initial energy starting point during the recharging of the input capacitor for the next firing sequence of the railgun.

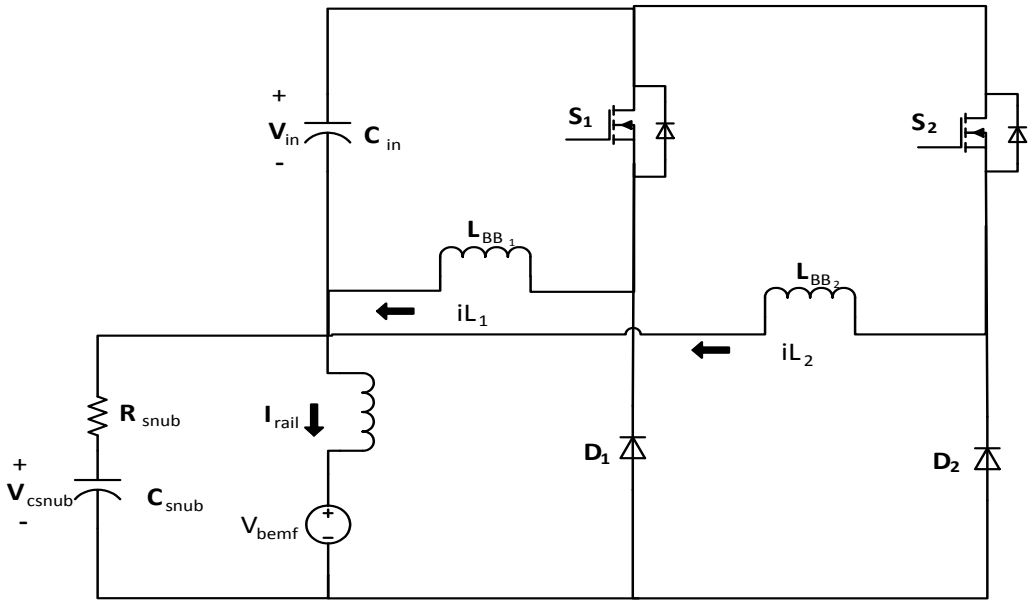

Figure 7. Buck-Boost Converter Schematic.

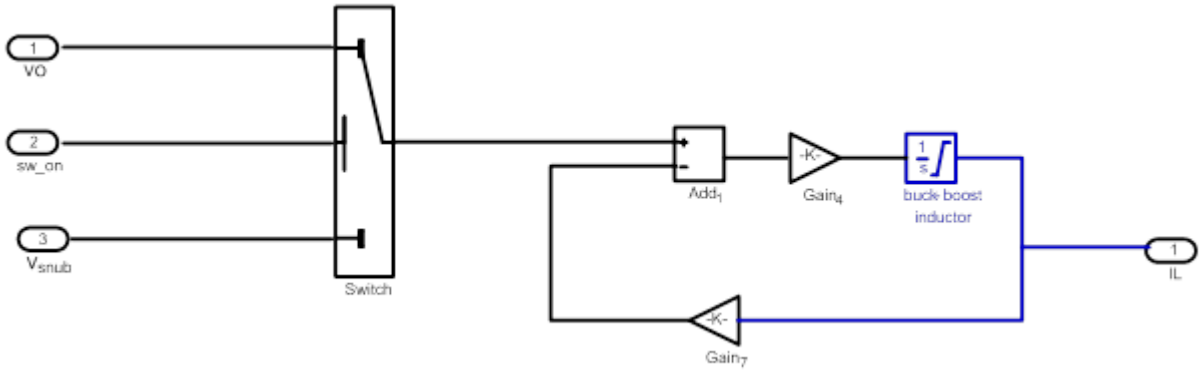

Figure 8. Simulink Model of Buck-Boost Circuit.

The control model used to control the current is shown in Figure 9. A PI closed control loop scheme is used in gating the switches for the buck-boost circuit models. The current from each of buck-boost converters is subtracted from a ramp reference current to create an error signal. The PI controller uses this error signal to generate a duty cycle signal. The control signal from the PI controller and a triangular wave signal for modulation, which is created using a triangular wave generator, are both sent to a comparator. The sampling and comparator circuit generates a square-wave control signal that is based on the characteristic of the signal from the PI controller. When the control signal is more positive than the triangular wave, a positive square-wave signal is generated. The width of the square-wave signal pulses determines the length of time that the switches are kept opened or closed. The output of the comparator is ANDed with a signal from a step-signal generator. The purpose of the step-signal generator is to allow the gating signal to pass for 8.0 ms and then be turned off. This signal is used as the gate-drive signal for the buck-boost converters. A ramp is used as the reference current to yield a constant current in the rails since the duty cycle of the switches varies during the shot.

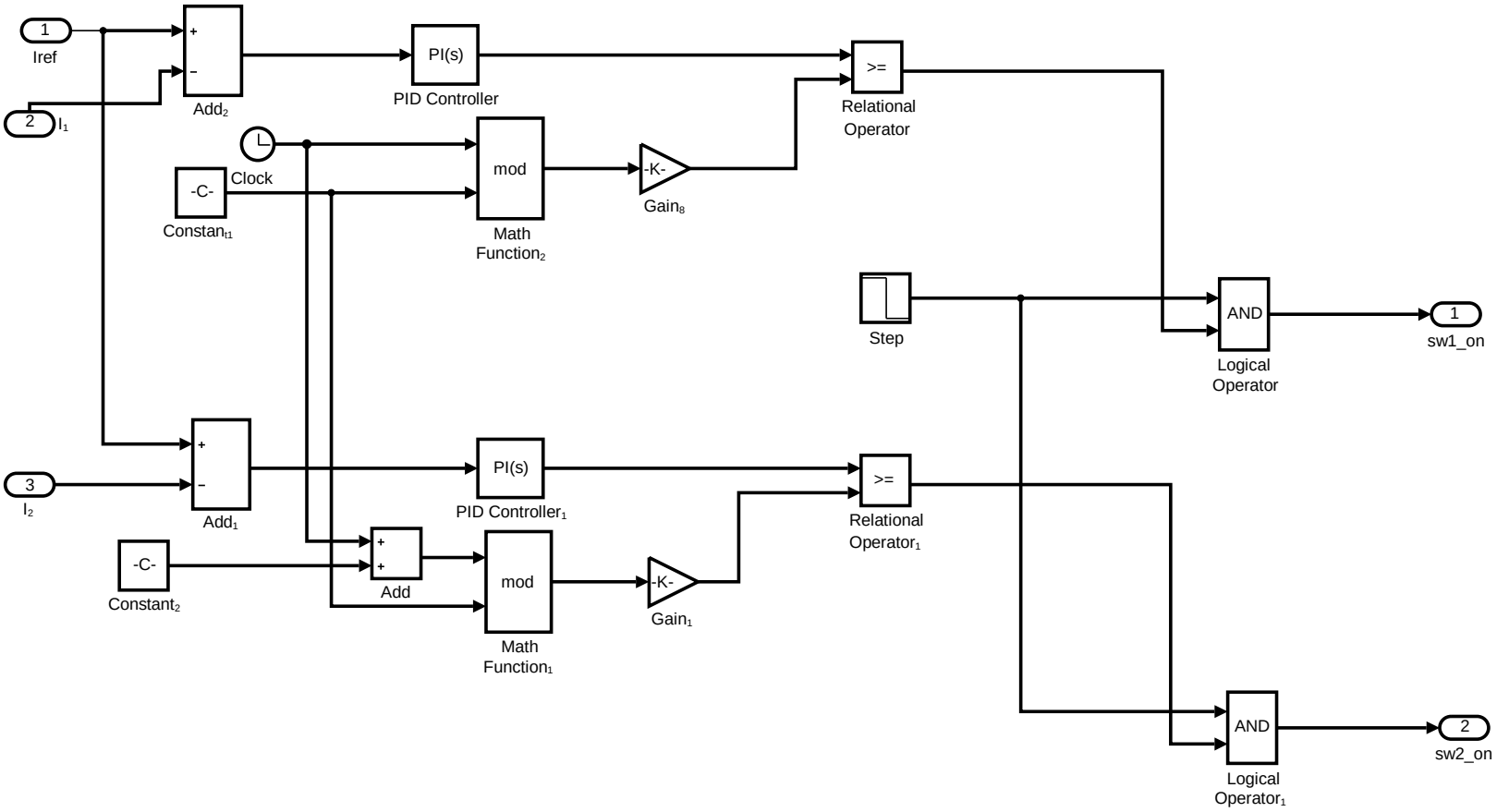

Figure 9. Gate Drive Circuit for Buck-Boost Controller.

III. RAILGUN SIMULATION WITH TWO DIFFERENT POWER SUPPLIES

The objective of this chapter is to highlight the Simulink modeling of the two different railgun power supplies and to provide a general overview of the equations used in the design. An accurate representation of the railgun model is essential to analyze and demonstrate the premise of this thesis.

Understanding the underlying differences between the efficiency of a thyristor PFN and a buck-boost converter PFN at delivering energy to the rails is essential in designing a railgun model. In illustrating this objective, we used Simulink to develop an equivalent railgun model, from which calculations for the post-fire transient energy of both circuits was determined. The model calculations provided a concrete comparison of the transient energy produced by both circuits after the projectile had exited the railgun. The railgun model also calculated the energy provided by each of the supplies, the velocity due to the Electromagnetic Force (EMF) and the characteristic of the projectile displacement over time. The Simulink model used to calculate the velocity and displacement of the projectile due to EMF is illustrated in Figure 10. The design parameters used in our simulation for a nominal naval railgun are also illustrated in Table 2.

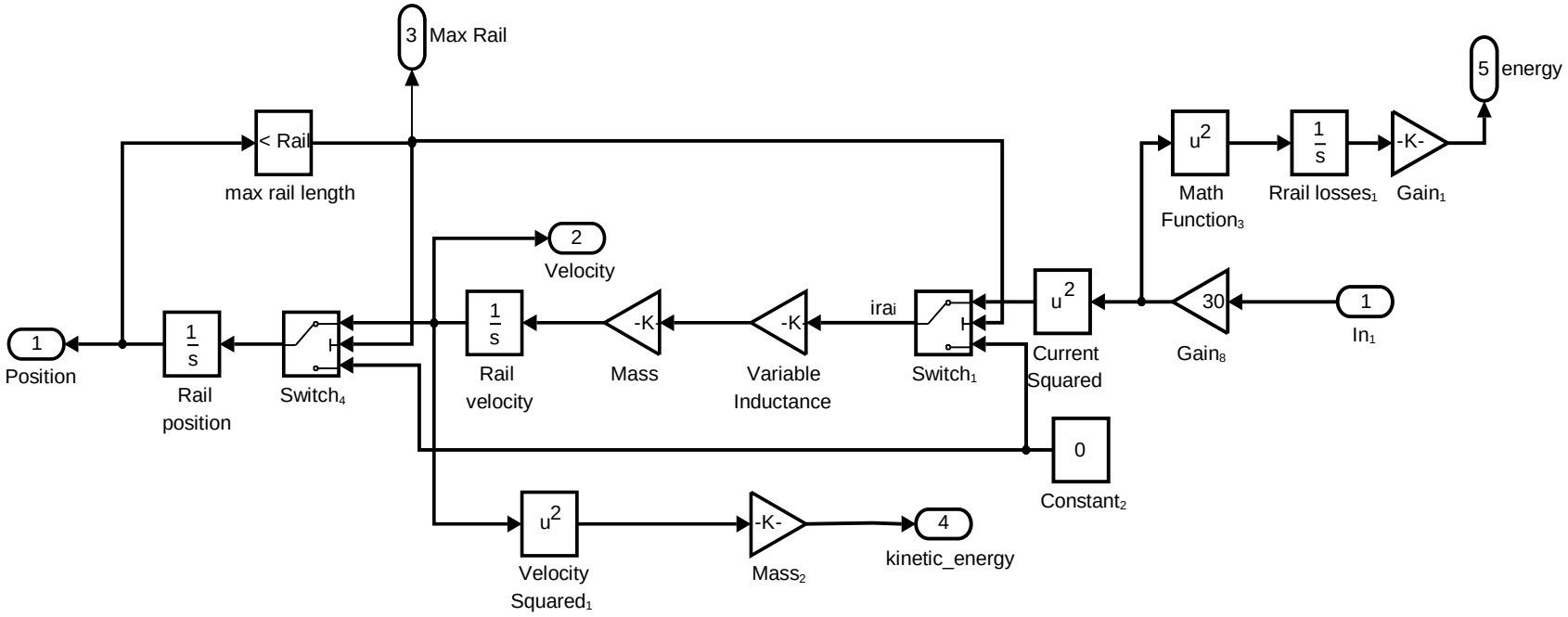

Figure 10. Component of Rail Model Used to Calculate Velocity, Acceleration and Position of the Projectile.

Table 2. Railgun Model Parameter.

Variable Name	Description	Value	Units
$\mathbf{C_{snub}}$	Capacitance of the snubber capacitor	20×10^{-5}	F
L'	Inductance gradient of the rail	5×10^{-7}	H/m
$\mathbf{L_{rail}}$	Inductance from the supplies to the armature when the transient begins	20×10^{-6}	H
m	Armature mass including projectile	3.125	kg
Rail	Length of the conducting portion of the rail	10	m
Rail space	Distance between the rails	500×10^{-3}	m
$\mathbf{R_{prime}}$	Resistance gradient of the rail	6×10^{-5}	Ω/m
$\mathbf{R_{snub}}$	Resistance in the snubber capacitor branch	0.05	Ω
$\mathbf{R_{20}}$	Resistance from the supplies to the armature when the transient begins	6×10^{-5}	Ω

The model for the proposed railgun load was constructed in Simulink using equation blocks that were used to calculate the various characteristics of a railgun. The model began with the summation of the two current sources from our buck-boost converters. The current signals were then used in calculating the snubber capacitor voltage V_{csnub}, shown in Figure 7, by multiplying the currents and the reciprocal of the snubber capacitance ($1/C_{snub}$) and then sending the computation to an integrator.

$$V_{CSnub} = \int \frac{I_C}{C_{Snub}} dt \,. \tag{18}$$

This snubber capacitor voltage is sent to an arithmetic block that computes the various voltage drops in the circuit. This is essential in calculating the change in rail current. The

snubber capacitor voltage and the voltage across the snubber resistor, labelled R_{snub} in Figure 7, in the model are added together. This snubber resistor voltage is calculated in the model by multiplying the current by the snubber resistance:

$$V_{RSnub} = I_c R_{snub} . \tag{19}$$

The voltage drop due to rail resistance and the voltage across the rail inductor and inductance gradient as a function of rail length is subtracted from the two snubber voltages. This calculation enables us to determine the change in the rail current as the projectile travels down the rails due to the EMF. The EMF acting on the circuit is based on the principle of Faraday's law of induction, which relates the EMF acting on a coil in a magnetic circuit and is proportional to the negative of the time rate of change of the magnetic flux due to its current. In our case, we have a coil of one loop, where the rails and armature complete the circuit between both rails. We calculate the electromagnetic force ε on the conducting armature from

$$\varepsilon = \frac{d\Phi_B}{dt} \tag{20}$$

where ε is the EMF induced on the conducting armature and Φ_B is the magnetic flux behind the armature. From this, we can calculate the rail current by identifying the constituents of the flux. The magnetic flux is related to the inductance formed by the area of the closed loop bounded by the armature, rails and the connecting power supply:

$$\Phi = (L_{rail} + x \cdot L^{'}) I_{rail} . \tag{21}$$

In (19) L_{rail} is the inductance due to the power supply and the closed loop formed by the armature and rails, L' is the inductance gradient of the rail, which is due to the geometry of the rails, and x is the length of the rails. Using (21), we can rewrite (20) so that the electromotive force is

$$\varepsilon = \frac{d}{dt}\left[\left(L_{rail} + x \cdot L^{'}\right) I_{rail}\right]. \tag{22}$$

If we differentiate, using the chain rule, we can solve for the rail current to get

$$\varepsilon = \left[\frac{d\left(L_{rail} + x \cdot L^{'}\right)}{dt} I_{rail} + \frac{dI_{rail}}{dt}\left(L_{rail} + x \cdot L^{'}\right) \right]. \tag{23}$$

The displacement x changes with time, which gives us the velocity of the armature v in m/s. In the second term on the right side of (23), we have the time rate of change of the rail current. We can derive the change in rail current from

$$\frac{dI_{rail}}{dt} = \frac{\left(\varepsilon - I_{rail} \cdot v \cdot L^{'}\right)}{\left(L_{rail} + x \cdot L^{'}\right)}. \tag{24}$$

By integrating (24), we get the rail current that is utilized in the simulation.

To analyze the post-fire energy dissipated in the rail, which is the energy due to the continued supply of current after the projectile exits the railgun, we constructed two separate models in Simulink. The first model is used to calculate the post-fire energy into the resistor in the railgun for both PFNs after the projectile exits the railgun. The second model calculated the energy contributing to the formation of an arc in the rails after the projectile exits the railgun. Our post-fire energy calculation was done by multiplying the current delivered by each of the respective supplies by the equivalent rail resistance as illustrated in Figure 11. The product of the delivered current and the rail resistance was sent to the third input of a three-input conditional switch. The first input of the switch is the simulated back EMF (BEMF), which is the expected BEMF characteristic of the railgun during the shot. The second input is an 8.0 ms timer that simulates the time at which the projectile has exited the gun. After 8.0 ms, the switch transitions from the BEMF signal to a resistor, and at this point we observed the post-fire behavior of both circuits. The second model of our simulation was the post-fire arc calculation for both circuits. The model used for the arc calculation is shown in Figure 12.

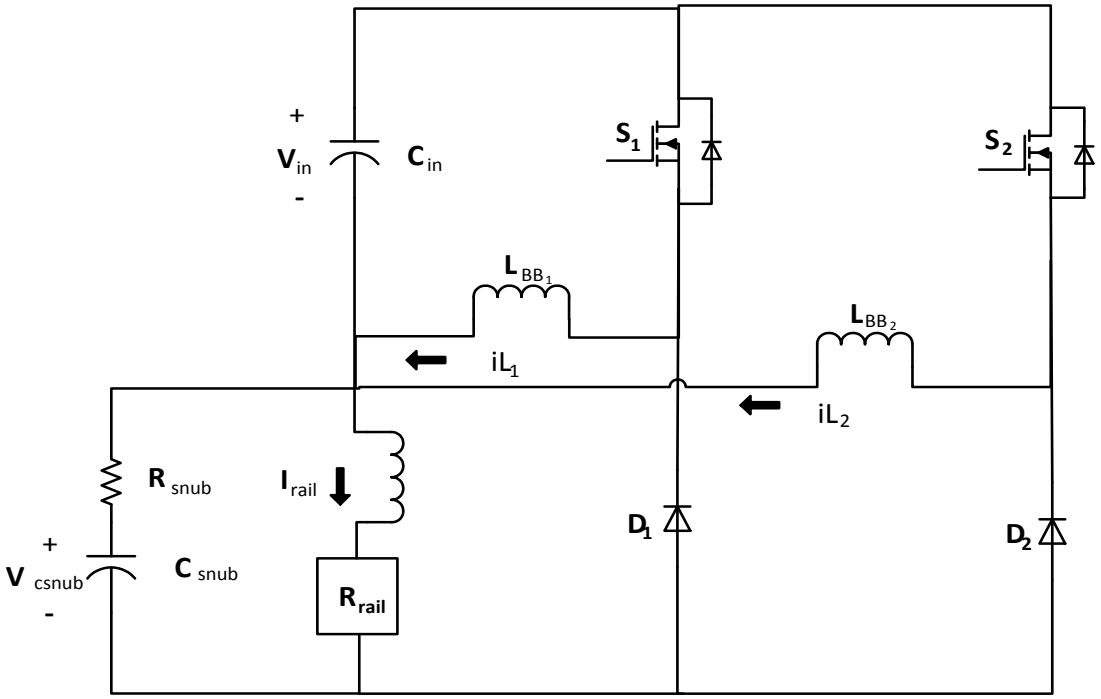

Figure 11. Equivalent Circuit Used to Quantify the Post-Fire Energy into the Resistor after the Projectile Exited the Railgun.

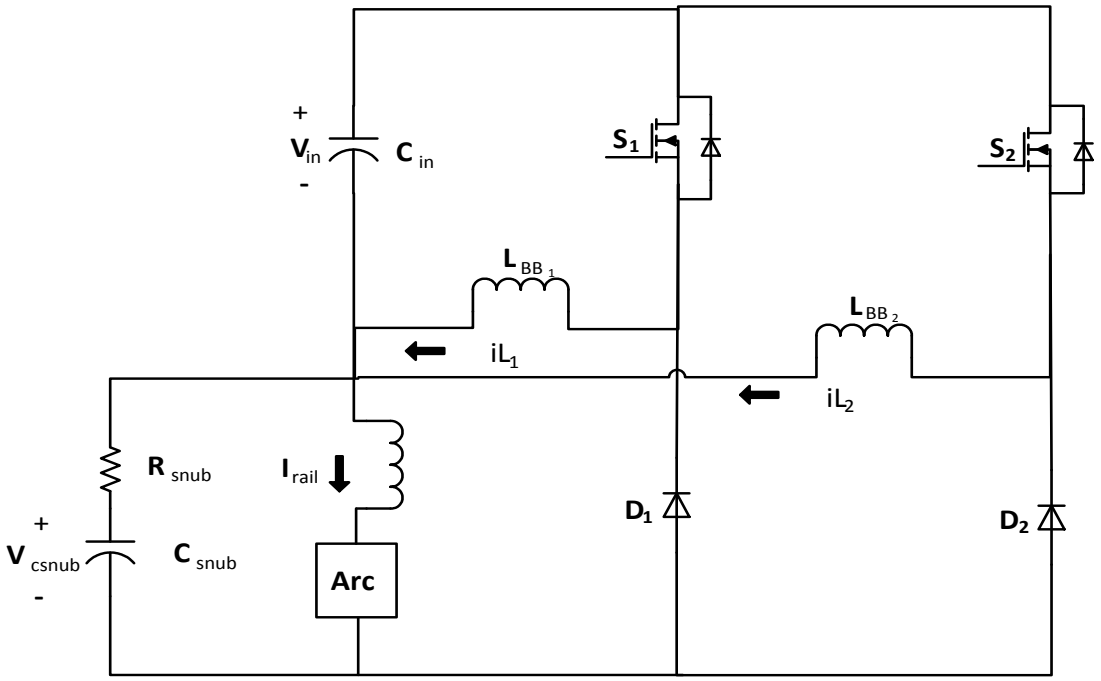

Figure 12. Equivalent Circuit Used to Quantify the Post-Fire Contributing to Arcing after the Projectile Exits the Rails.

Computations were done on the voltage, current and resistance associated with arcing in [6] and [7]. This publication provided a comprehensive view on calculating arcing between two electrodes in terms of current, voltage and resistive properties. The arc between two electrodes in open air has a current-voltage (I-V) characteristic that is inversely related. We can calculate the voltage V_{arc} and arc resistance R_{arc} in relation to the current I_{arc} from [6]

$$V_{arc} = \left(20 + 0.534 z_g\right) I_{arc}^{0.12}, \tag{25}$$

and

$$R_{arc} = \frac{20 + 0.534 z_g}{I_{arc}^{0.88}}, \tag{26}$$

respectively.

In (25) and (26), z_g is the spacing in mm between two electrodes or, in this case, the spacing between both rails [6]. The minimum I_{arc} necessary to form an arc is [6]

$$I_{arc} = 10 + 0.2 z_g . \tag{27}$$

Using these equations, we derived our Simulink model to quantify the post-fire energy in the rails that contributed to the formation of arcs. This post-fire arc energy was quantified by calculating the arc-voltage, which is done in the Simulink model for both the buck-boost and thyristor circuits. Next, we multiplied that arc-voltage by the arc current I_{arc}, which is the rail current in this case, and then integrated over the time period of the simulation. The arc-voltage calculation used in our Simulink model is shown in Figure 13. The arc energy is shown in Figure 29 from chapter IV.

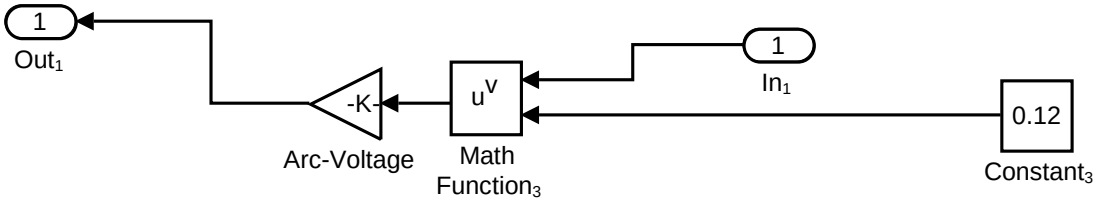

Figure 13. Arc Voltage Calculation Model.

The equations used in the modeling of the rail system enable us to calculate the velocity and position of the projectile throughout the duration of a shot. The velocity calculation allowed us to calculate the kinetic energy in the projectile for the current delivered to the rails by each of the respective PFNs. From plotting the velocity of the armature, we determined that the characteristics of the plot was due to the shape of the current delivered by each of the respective supplies. The model used to calculate the velocity and position of the projectile was based on [5]

$$\frac{d^2x}{dt^2} = \frac{dv}{dt} = \frac{L'I^2}{2m} \rightarrow \iint d^2x = \int dv = (L' I / 2m) \int Idt \tag{28}$$

and

$$x = \left(\frac{m}{L'}\right)\left(\frac{v}{I}\right)^2 \rightarrow v = I\left(\frac{L'x}{m}\right)^{\frac{1}{2}}, \tag{29}$$

which describes the acceleration of a projectile in railgun due to electromagnetic forces, respectively. In (28) and (29), x is the position in m and v is the velocity in m/s.

From (28) and (29) we plotted the velocity characteristics as a function of the current supply from both circuits.

A. THYRISTOR PFN

In analyzing the differences between the buck-boost converter power supply and the thyristor power supply, it is necessary to understand the behavior of the energy supplied to the railgun and the characteristics of the transfer of that energy to the armature. In this section, we illustrate the behavior of the energy delivered to the rails by

the thyristor circuits and calculate the armature velocity. We also quantify the amount of energy transferred to the armature from the thyristor circuit.

The thyristor PFN supplies current to the rails from a series of sequentially-discharging capacitor banks. The number of capacitors and capacitor sizes are based on the desired projectile speed and kinetic energy. Our thyristor PFN is modeled in Simulink using three thyristor circuits. Two of the circuits are supplied by a 6.0-mF capacitor, and the third circuit is supplied by a 9.0-mF input capacitor. The distinction in capacitor size was to help shape the current. All three input capacitors are charged to 7.0 kV. Each capacitor in the circuits discharged for about 3.5 ms in sequential order. The sequential capacitor discharging produced a nonlinear current characteristic. To produce a desirable velocity, we multiplied the current delivered to the railgun from the supply by 30 in our railgun model. This nonlinear shape of the thyristor circuit current characterizes the shape of the current delivered to the railgun. The shape of the thyristor current to the rails is shown in Figure 14. If we increase number of smaller capacitors in the circuit, thereby decreasing the RC time, we can discharge the capacitors at a much faster rate. This increases the linearization of the current but also increases the number of capacitors needed to produce the desired rail energy.

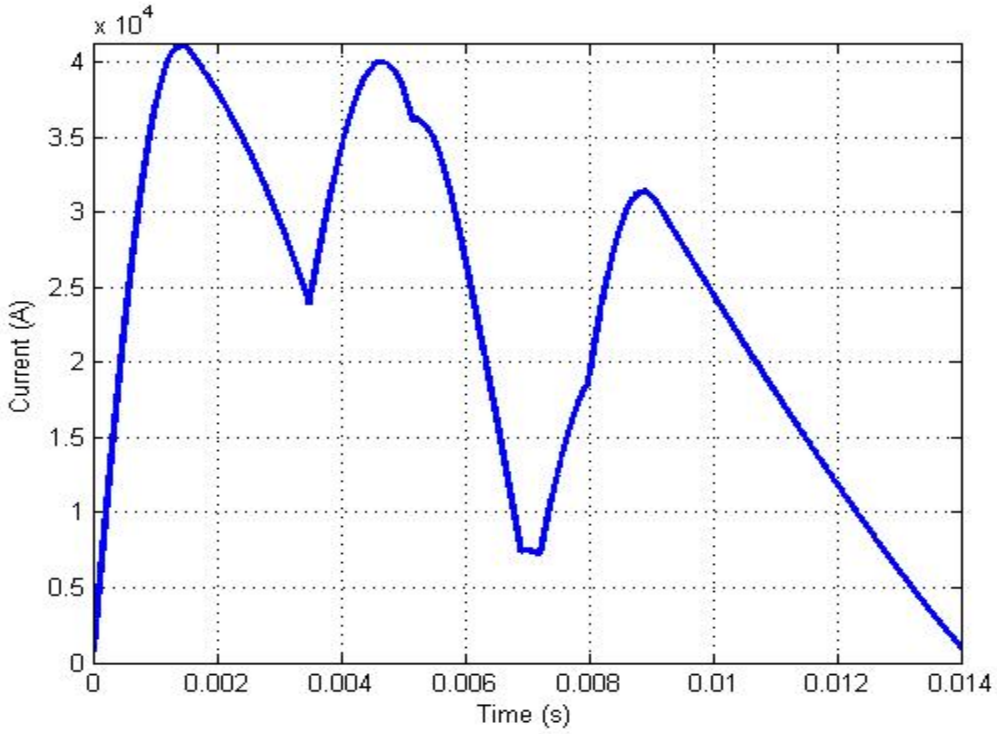

Figure 14. Shape of the Current Delivered by the Thyristor Circuit to the Railgun Model in Simulink.

The nonlinear characteristic of the current delivered to the rails by the thyristor PFN, represented in Figure 14, provides some general inferences of the shape of the energy delivered to the rails and the characteristics of the armature velocity. The plot of the armature velocity as a function of time is illustrated in Figure 15.

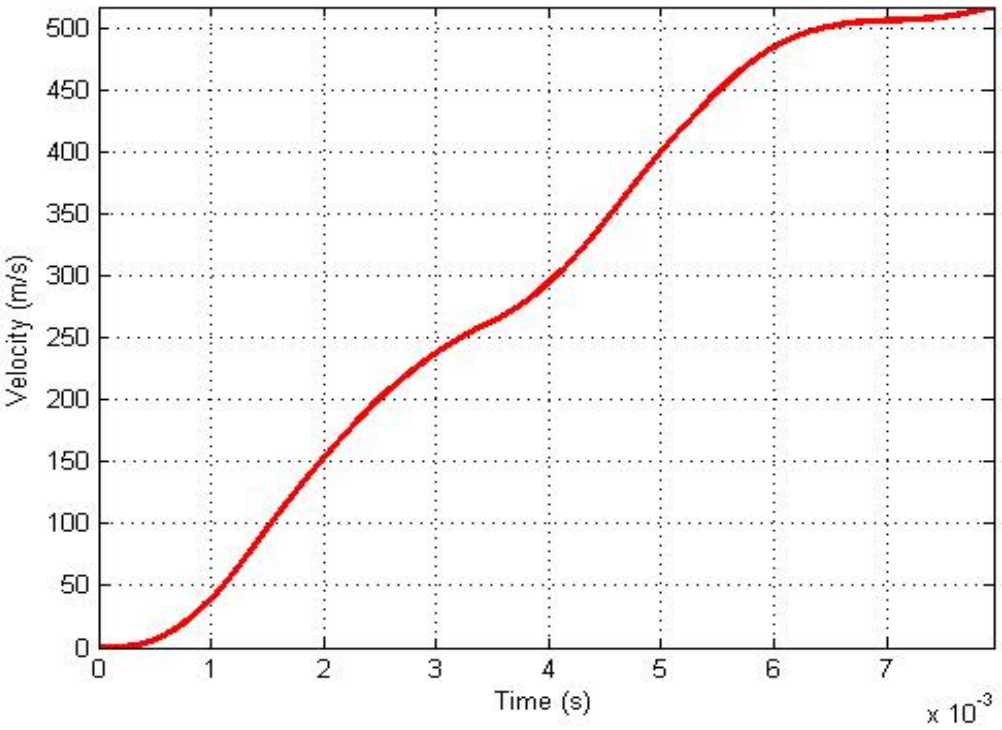

Figure 15. Velocity of the Armature Due to the Energy Delivered from the Thyristor PFN.

The shape of the armature velocity is characterized by the nonlinear behavior of the current from the thyristor PFN. Between 6.0 and 8.0 ms, just before the armature exits the rails, we have little to no change in the velocity as shown in Figure 15. This is due to the corresponding time gap of the current plot, where a large time gap exists between the discharging of the last two capacitors. This contributed less overall energy to the rails. The armature velocity increased slightly to 522.6 m/s just before exiting the rails; this increase in velocity correlates to the discharging of the final capacitor in the circuit.

The energy transferred from the supply to the projectile can be determined by calculating the kinetic energy of the armature, which is based on its velocity. Our railgun model gives the velocity of the projectile as a function of the delivered current from the supply and the armature mass. The energy transferred to the projectile by the thyristor is the velocity squared times the mass divided by two. We can compare the armature kinetic energy to the energy delivered from the supply by integrating the supply current times the

capacitor voltage over the duration of time. The comparison of the energy delivered from the thyristor circuit and the energy transferred to the projectile is shown in Figure 16. Simulated results show that the energy delivered to the rails from the thyristor circuit is 0.517 MJ. The energy transferred to the armature/projectile is 0.419 MJ and corresponds to 81 percent of the energy from the rails transferred to the armature. The remaining 19 percent is stored in the magnetic field that opposes the acceleration of the armature through the rails and as heat in the rails.

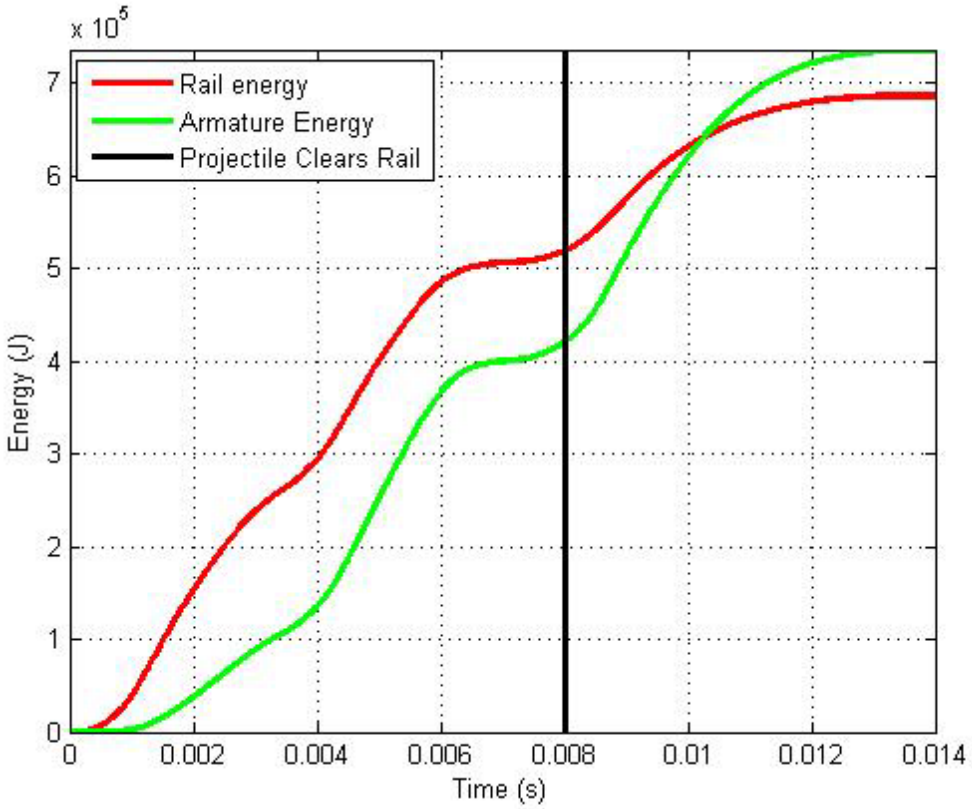

Figure 16. Rail Energy and Energy Transferred to Armature.

B. BUCK-BOOST PFN

The buck-boost converter PFN delivers a relatively constant current to the rails. This current is regulated by the duty cycle set by the PI controller. The current from the buck-boost converter is fed back to the PI controller. The controller matches the converter current to the demand of the load by regulating the duty cycle for both converters. The ability to control the current being delivered to the rails by regulating the duty cycle for the duration of time the armature is in the rails is critical in maintaining a constant rail current. The current delivered by each of the buck-boost converters is shown in Figure 17.

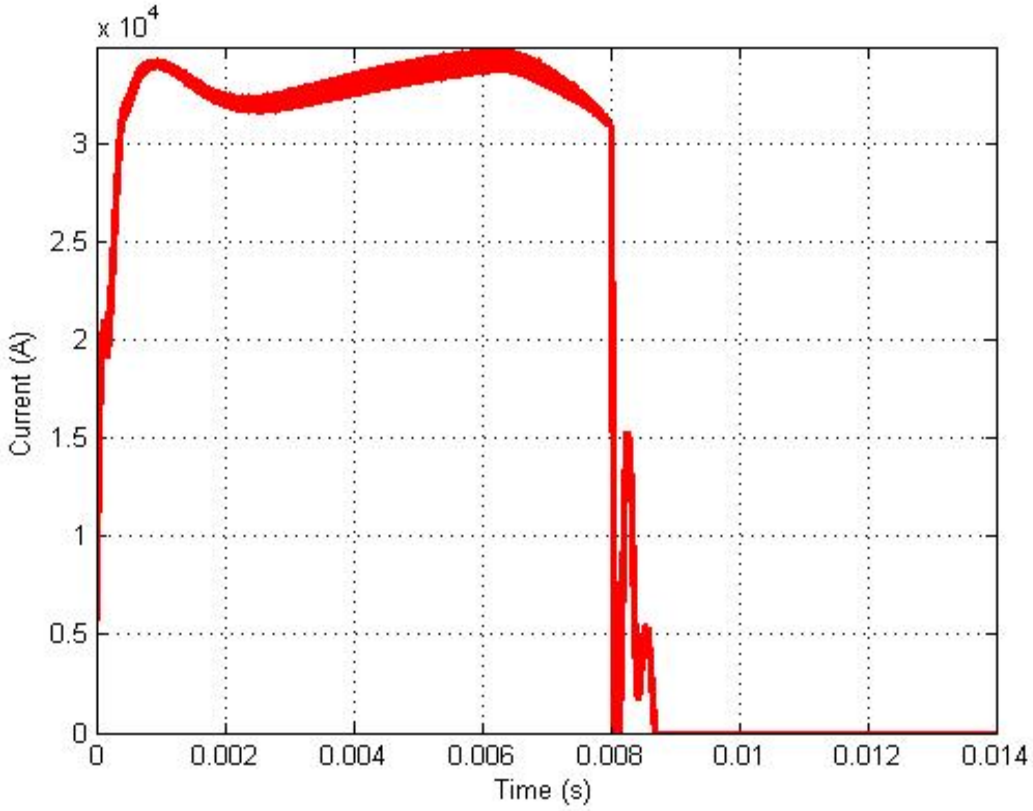

Figure 17. Buck-Boost Converter Supply Current.

The current plot in Figure 17 shows a rapidly increasing current to a peak of 34.27 KA at 0.9 ms. This current remained relatively constant until the armature had traveled to the end of the rails' length, where it is then regulated off by the PI controller. When we increase the buck-boost PFN modules to 30, thereby increasing the rails current 30 times levels previously demonstrated, we produce a linear armature velocity with a peak of 506.9 m/s at 7.99 ms.

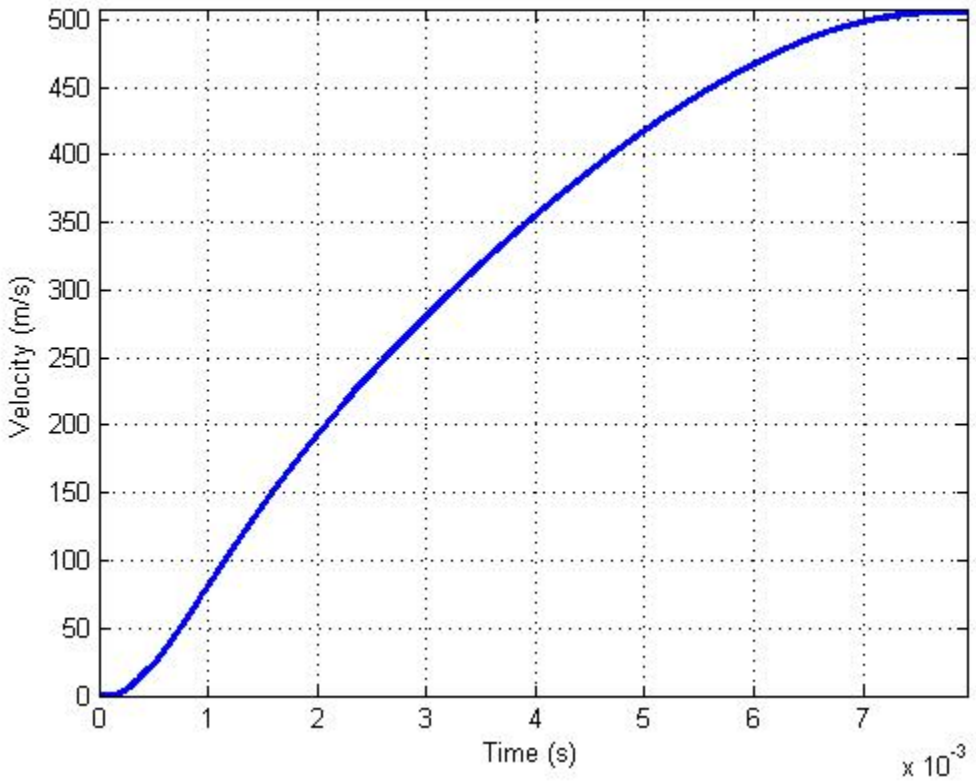

Figure 18. Armature Velocity Due to Current Delivered by the Buck-Boost Converter PFN.

The energy transferred to the armature due to energy delivered by the buck-boost PFN was determined similarly to the thyristor PFN as mentioned in the previous passage. We calculated the armature's kinetic energy based on the velocity calculation determined in the railgun model. The relationship between the railgun's energy delivered from the buck-boost PFN and energy transferred to the accelerating armature is shown in Figure 19. The calculated energy delivered from the buck-boost converters was 0.506 MJ. The

energy transferred to the armature was 0.401 MJ, approximately 80 percent of the total energy delivered to the railgun by the buck-boost PFN.

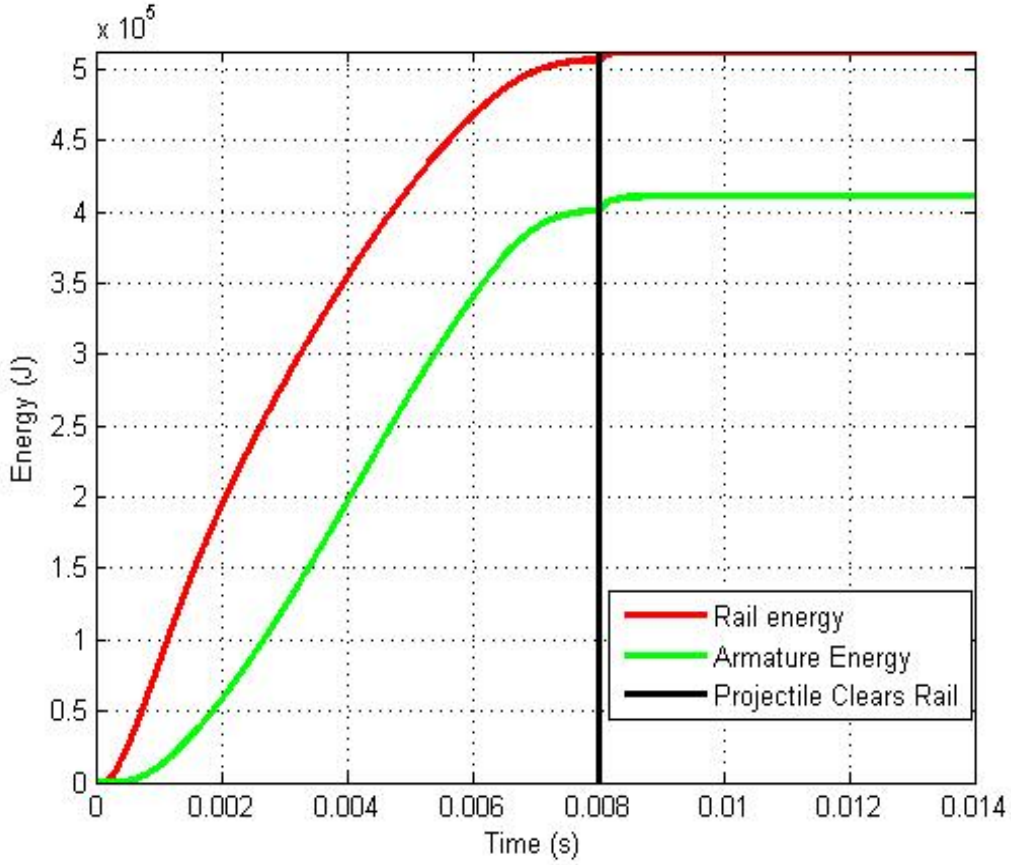

Figure 19. Buck-Boost PFN Rail Energy vs. Armature Energy.

A comparison between the armature energy and the energy delivered by both buck-boost converter and thyristor circuit shows the different characteristics of each PFN. From Figure 20, we see that the shape of the buck-boost rail energy is relatively linear in comparison to the thyristor circuit's energy plot up to the point at which the projectile exits the rails. From Figure 20, the thyristor energy is slightly higher than the buck-boost's energy right before the armature exits the railgun. This correlates to a 37.1 kJ over the buck-boost converter circuit. The energy differences show that a higher percent of the input capacitor's energy is delivered to the rails by the thyristor circuit than the

buck-boost converter. A comparison of the differences in armature kinetic energies with respect to energy by the respective PFNs is illustrated in Figure 21.

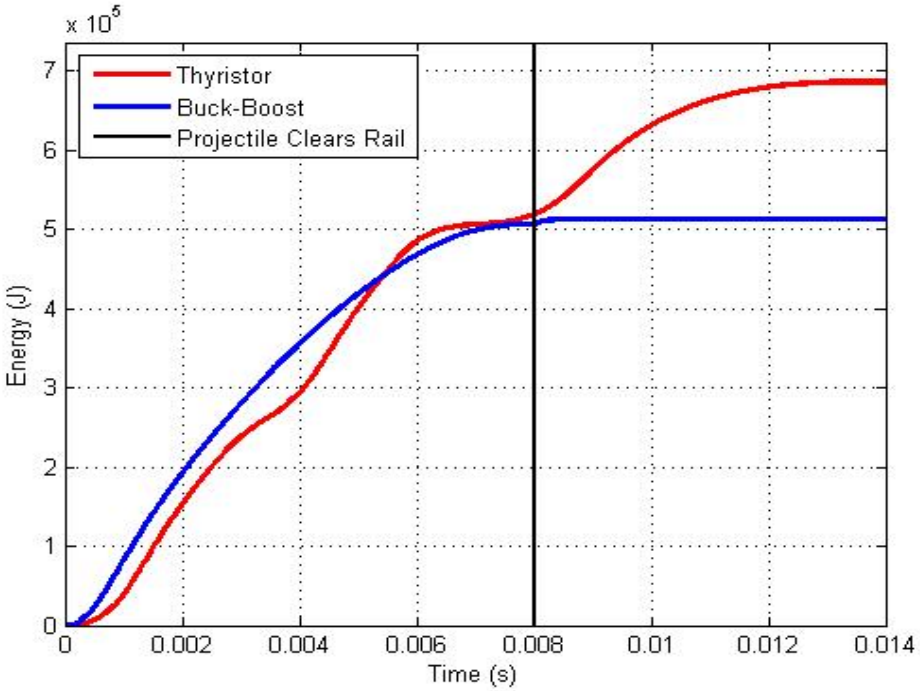

Figure 20. Buck-Boost and Thyristor Rail Energy vs. Time.

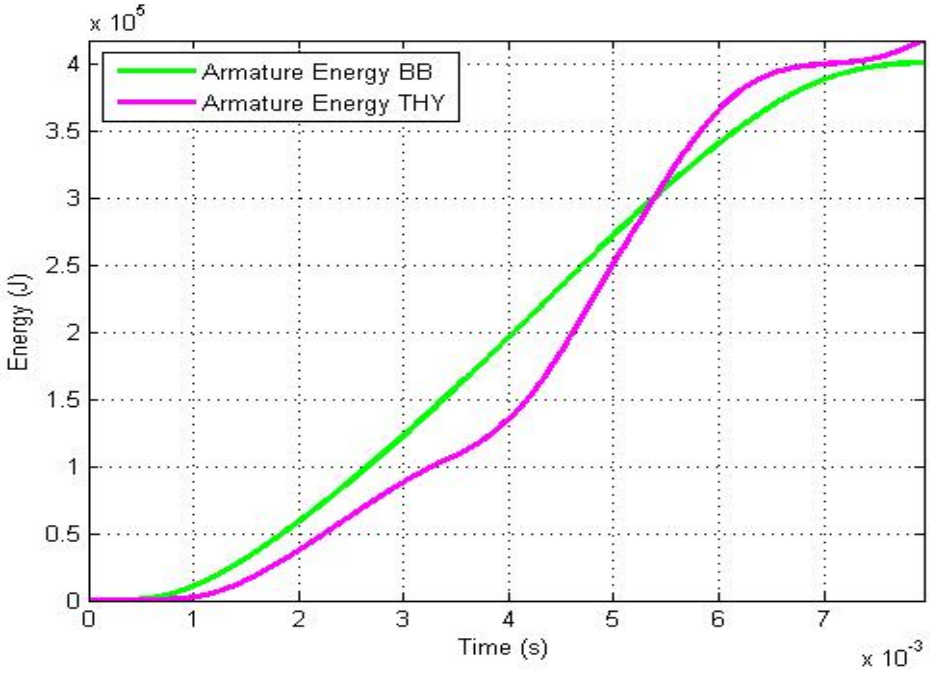

Figure 21. Armature Energy due to Buck-Boost and Thyristor PFNs.

A comparison between the thyristor railgun PFN and the buck-boost converter PFN is shown in Table 3. Starting with the same initial capacitor voltage, we see that the energy delivered to the rails by the thyristor circuit is 37.1 kJ larger than for the thyristor circuit. This slightly larger thyristor rail energy contributed a 15.3 m/s higher armature speed than the armature associated with the energy delivered by the buck-boost converter. Our railgun modeling revealed that thyristor circuit utilizes a higher percent of the energy in the input capacitor than the buck-boost converter circuit; this correlates to a slightly higher armature velocity and kinetic energy.

Table 3. Nominal Railgun Values for Both Buck-Boost and Thyristor PFN.

Variable	**Buck-Boost**	**Thyristor**	**Ratio**
Rail Energy	0.506 MJ	0.518 MJ	0.98
Armature Energy	0.401 MJ	0.419 MJ	0.96
Muzzle Velocity	506.4 m/s	518.1 m/s	0.98

THIS PAGE INTENTIONALLY LEFT BLANK

IV. RAILGUN POST-FIRE ENERGY

The objective of this chapter is to quantify the post-fire energy and compute the arc voltage and the energy associated with the formation of an arc within the railgun based on the energy delivered by both the buck-boost converter and the thyristor circuit. The post-fire energy, or muzzle flash, that occurs in the gun when the armature exits the railgun is detrimental to the life of the rails. The high current that forms at the muzzle of railgun when the projectile exits the rail creates a large amount of heat; this high temperature erodes the rails after each shot. The accumulation of rail thermal damage limits the number of shots possible for a given set of rails. The large current that forms when the armature exits the rails is mostly due to the loss of the low-voltage electrical contact between the armature and the rails. When the armature exits the railgun, the system inductance forces current through the rails, which results in a high-energy discharge in the form of arcing and heat. This discharged post-fire energy is calculated from [5]

$$W_e = \frac{LI^2}{2} \tag{30}$$

where W_e is the post-fire energy, L is the system inductance and I is the rail current.

Many solutions have been proposed for the suppression of muzzle flash in a railgun. One such solution proposed in [8] for suppressing the muzzle flash is to install a capacitor muzzle-shunt suppressor at the muzzle of the railgun. An alternative solution we propose in this thesis is not to necessarily address the arcing problem directly but rather address the root cause of the problem. The post-firing in the rails energy is due to the continuous flow of current to the rails well after the projectile has exited the railgun. We can eliminate this post-fire energy by stopping the supply of current to the rails immediately after the projectile exits the rails.

The existing thyristor based railgun power supply topology provides no means of controlling the current being delivered to the rails. For this reason, we cannot stop the discharge of energy to the rails. As a result, there is a great deal of inductive arcing and

heating at the muzzle. The proposed buck-boost converter topology enables control of the current being deliver to the rails. By controlling the current, we can stop the supply of current to the rails when the projectile exits the railgun, minimizing the post-fire muzzle flash.

A. THYRISTOR POST-FIRE ENERGY ANALYSIS

In our efforts to quantify the post-fire energy for both power supply topologies, we developed two distinct models in Simulink to quantify the post-fire energy and the energy contributing to the formation of arcing within the rail. To calculate the post-fire energy for the thyristor circuit from the model, we square the thyristor rail current after 8.0 ms; this is the estimated time when the projectile exits the rails. The current squared is multiplied by the equivalent rail resistance of 0.030 Ω and then integrated. Results from the post-fire energy model calculation reveal that the total energy dissipated in the rails after the projectile exits the rail is 0.1265 MJ. This is the change of the energy starting at 8.0 ms to the moment when the current is zero. Figure 22 is a plot of the rail energy due to the energy delivered by the thyristor PFN. At 8.0 ms, the projectile clears the rails, but the energy in the rails continues to increase after the shot.

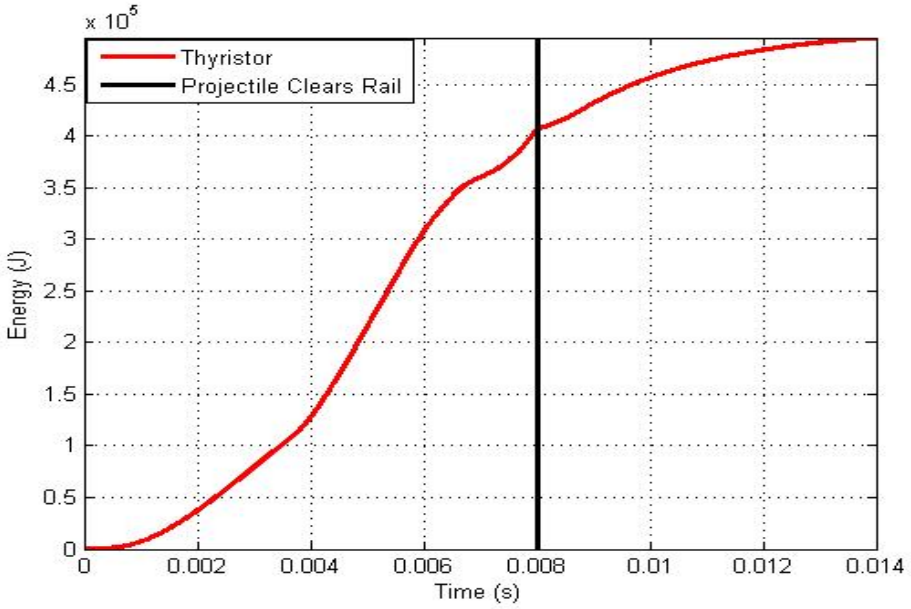

Figure 22. Thyristor Rail Energy vs. Time.

The continued delivery of energy to the rails after the projectile exits is due to the continuous discharge of the circuit input capacitors and the energy stored in the inductance. At 6.8 ms, the third input capacitor begins discharging, at 8.0 ms the projectile exits the rails. At this point, the input capacitor still has about 60 % of its initial energy. The capacitor continues to discharge until it reaches 0.0 V, contributing to the energy in the arc. This is illustrated in Figure 23 and Figure 24.

The plot of the post-fire energy delivered to the rails is shown in Figure 23, where at 8.0 ms the armature exits the rail, but the energy in the rail continues to increase to a peak of 0.496 MJ. The current contributing to this energy is presented in the Figure 24. When we observe the rail current at 8.0 ms, the current continues to flow to the rail. The current delivered to the rails by the thyristor circuit after the armature exits the rails is 20.0 kA.

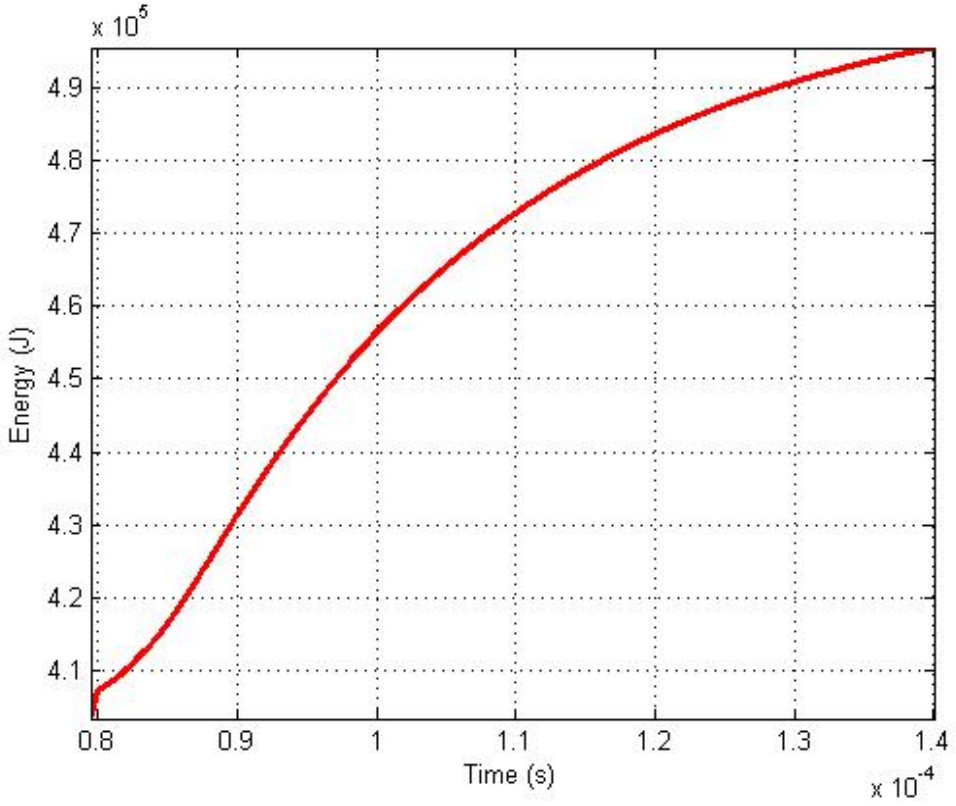

Figure 23. Thyristor Post-Fire Energy vs. Time.

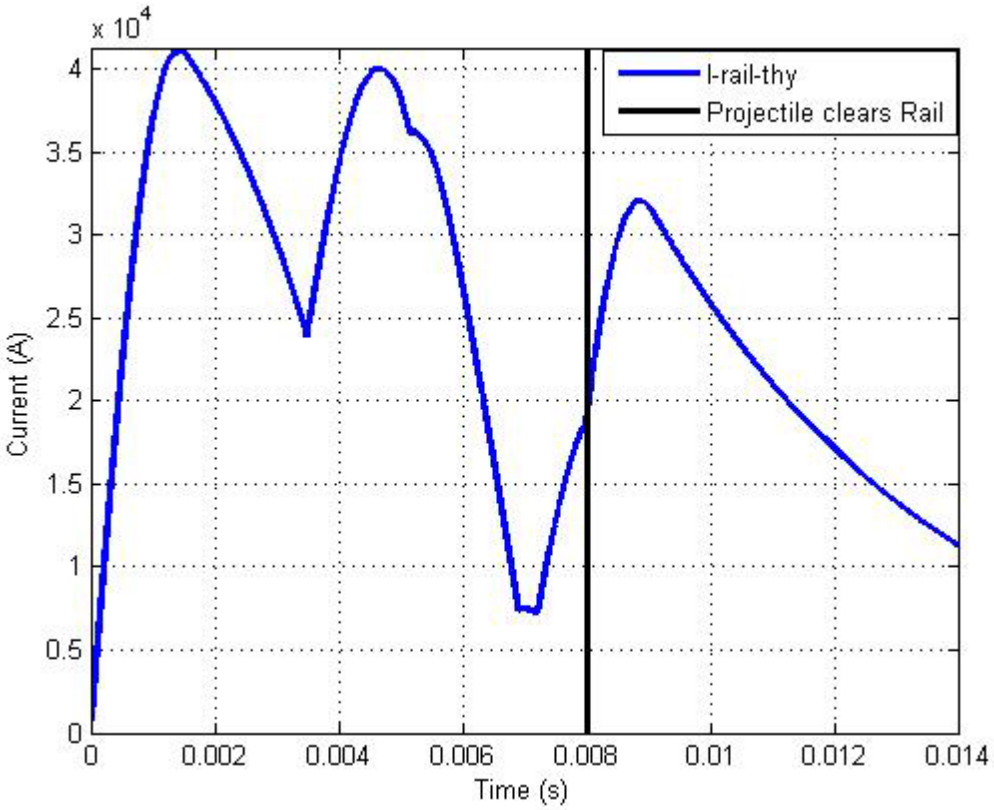

Figure 24. Thyristor Rail Current.

B. BUCK-BOOST CONVERTER POST-FIRE ENERGY

In our simulation, we compare and quantify the energy delivered to the railgun after the projectile left the rails for two different circuits. We developed a Simulink model similar to that of the thyristor pulse-forming network for the buck-boost converter. In the model, we analyzed the current delivered to the rail by the buck-boost converter to observe the characteristic of the current and to quantify the resulting energy.

In our effort to quantify the post-fire energy delivered to rails by the buck-boost converter, we plotted the rail current to understand the characteristic of the current delivered after the projectile had left the rails. The sum of the two inductor currents, L_{BB1} and L_{BB2}, during the entire shot is shown in Figure 25. The current in L_{BB1} and L_{BB2} flows into the arc after the projectile leaves the railgun. From the plot illustrated in Figure 25, after 8.0 ms the projectile exits the rails. After 8.0 ms, a slight ripple current due to RC components is delivered to the railgun; this transient ripple current quickly decays to

zero. As shown in Figure 25, between 6.5 and 8.0 ms the current rapidly decays, and after 8.0 ms the buck-boost switch is turned off. At this point, the input capacitor is no longer delivering energy to the railgun, unlike the thyristor current. This post-fire rail current is primarily due to the continuous conduction of the supply inductor and voltage reversal across the diodes.

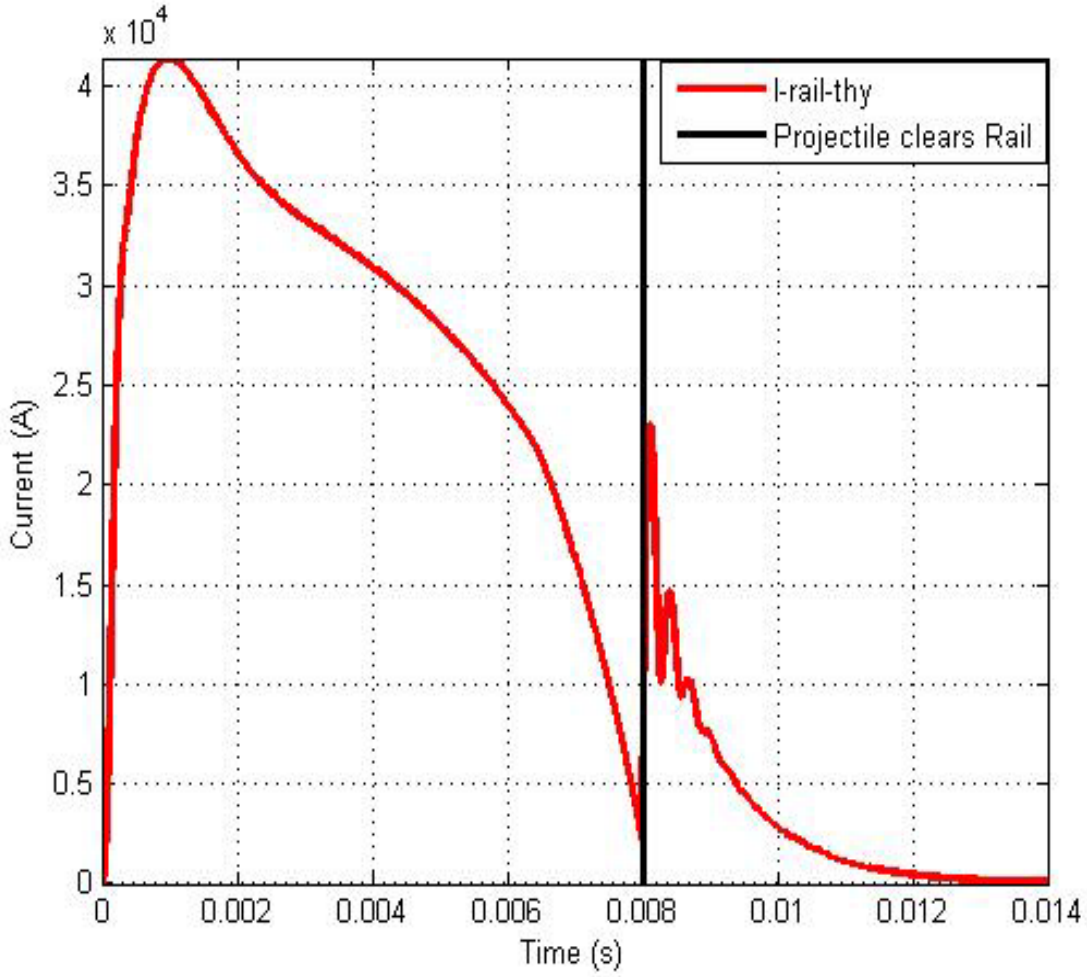

Figure 25. Buck-Boost Converter PFN Rail Current.

The post-fire energy delivered by the buck-boost PFN is shown in Figure 27. From Figure 26 and 27, we observe that the energy in the rail increased from 0.38 MJ to 0.3855 MJ between 8.0 to 14.0 ms, contributing a total 5.50 kJ of energy. From our analysis, the post-fire energy due to the buck-boost converter circuit is substantially less than the thyristor circuit. This energy can be additionally reduced with a more finely tuned model.

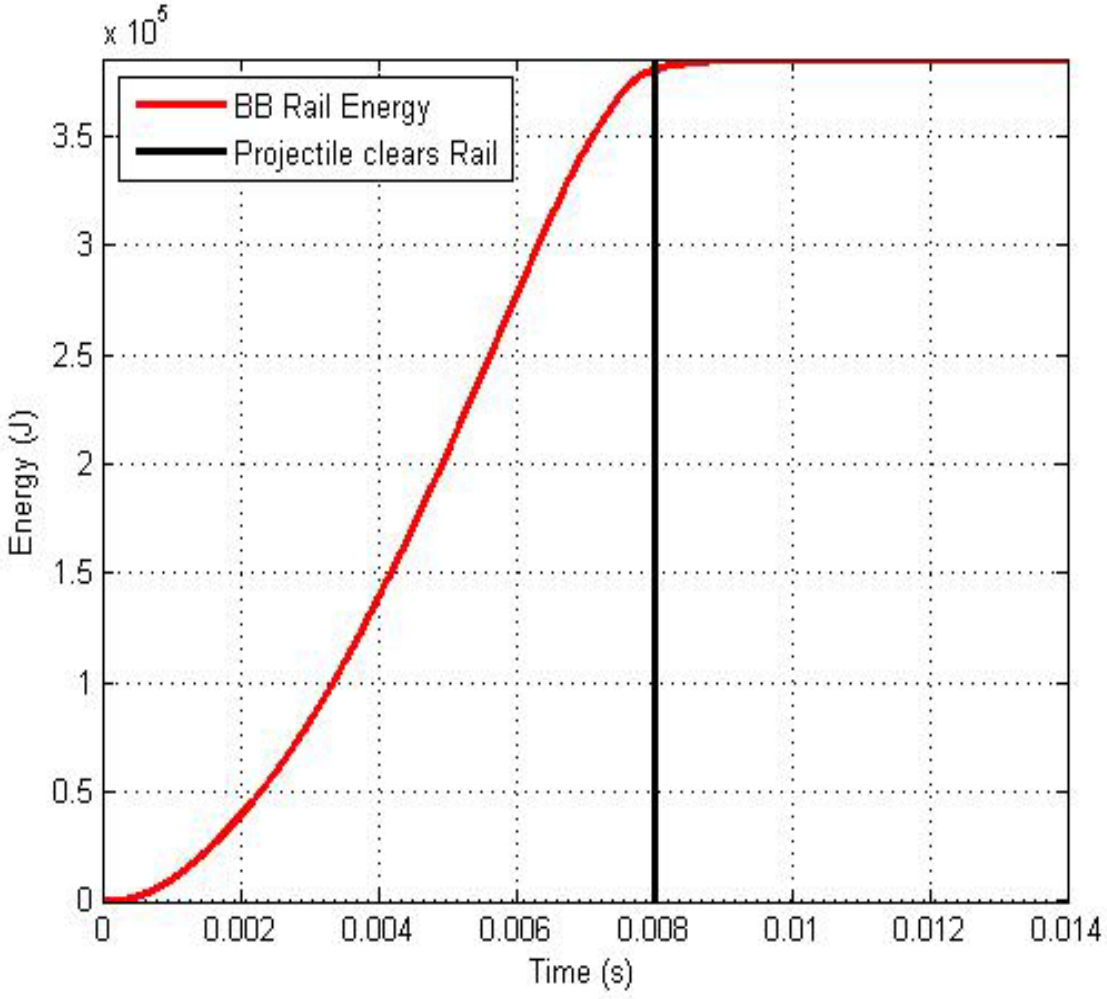

Figure 26. Buck-Boost Converter Rail Energy.

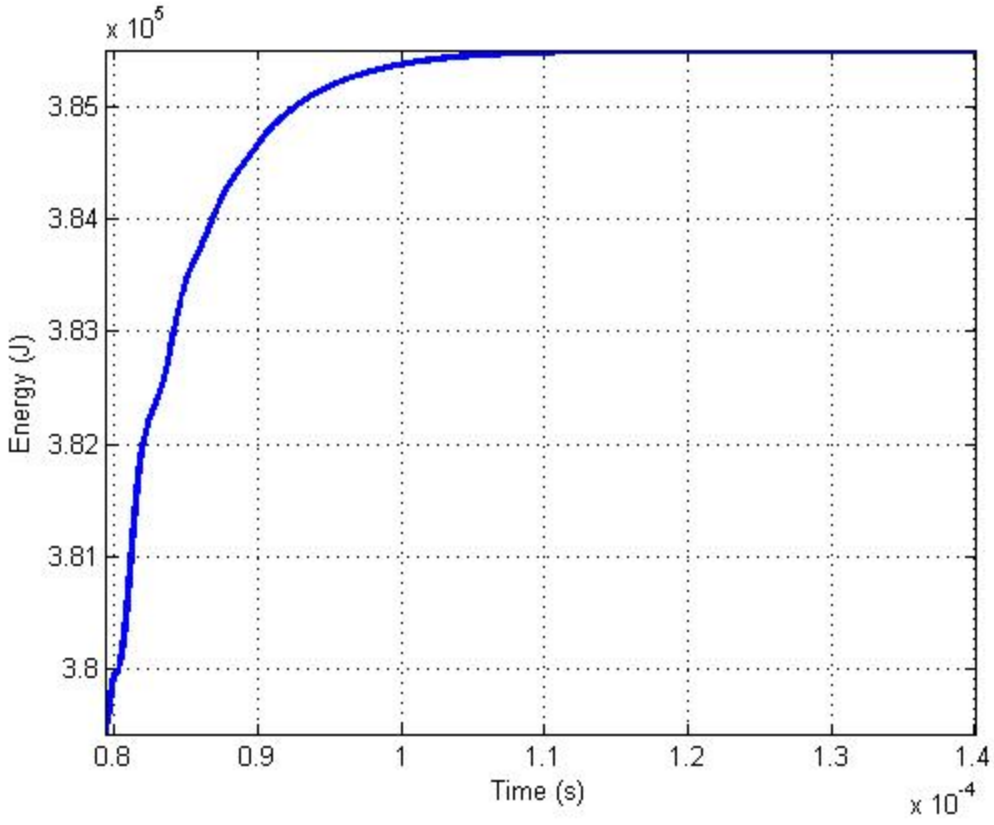

Figure 27. Buck-Boost Converter Post-Fire Energy.

C. POST-FIRE ARC AND ENERGY

Muzzle flash in the railgun after the projectile exits the rails is primarily due to the post-fire arcing that occurs when the armature exits the rails. In the previous two sections, we looked at the arc energy by representing the arc with a 30-mΩ resistor. To get a sense of the severity of the muzzle flash, or the amount of the energy that contributes to the formation of arcs, we generated a Simulink to model to calculate the arc current and arc energy for the buck-boost PFN and the thyristor PFN, respectively, using an arc mode [6]. The simulation for both supplies outlined the areas in which the buck-boost converter shows promise over the thyristor circuit. By plotting the arc current and energy for both circuits, we are able to quantify the differences between the two.

Simulated data of the post-fire energy in the form of arcing, which is based on arc current and voltage equations described in previous chapters, revealed that the post-fire arcing between the rails was substantially less for the buck-boost converter circuit when

compared to the thyristor circuit. The post-fire arc current for the buck-boost converter exists in the rails for a very short period after the projectile exits the rails. As a result, arcing in the rails extinguished 0.789 ms after the projectile exits the rails. Comparatively, the thyristor arc current lasted 6.0 ms longer than the buck-boost converter. The arc current and arc energy for both the buck-boost converter and the thyristor circuit are shown in Figure 28 and Figure 29, respectively.

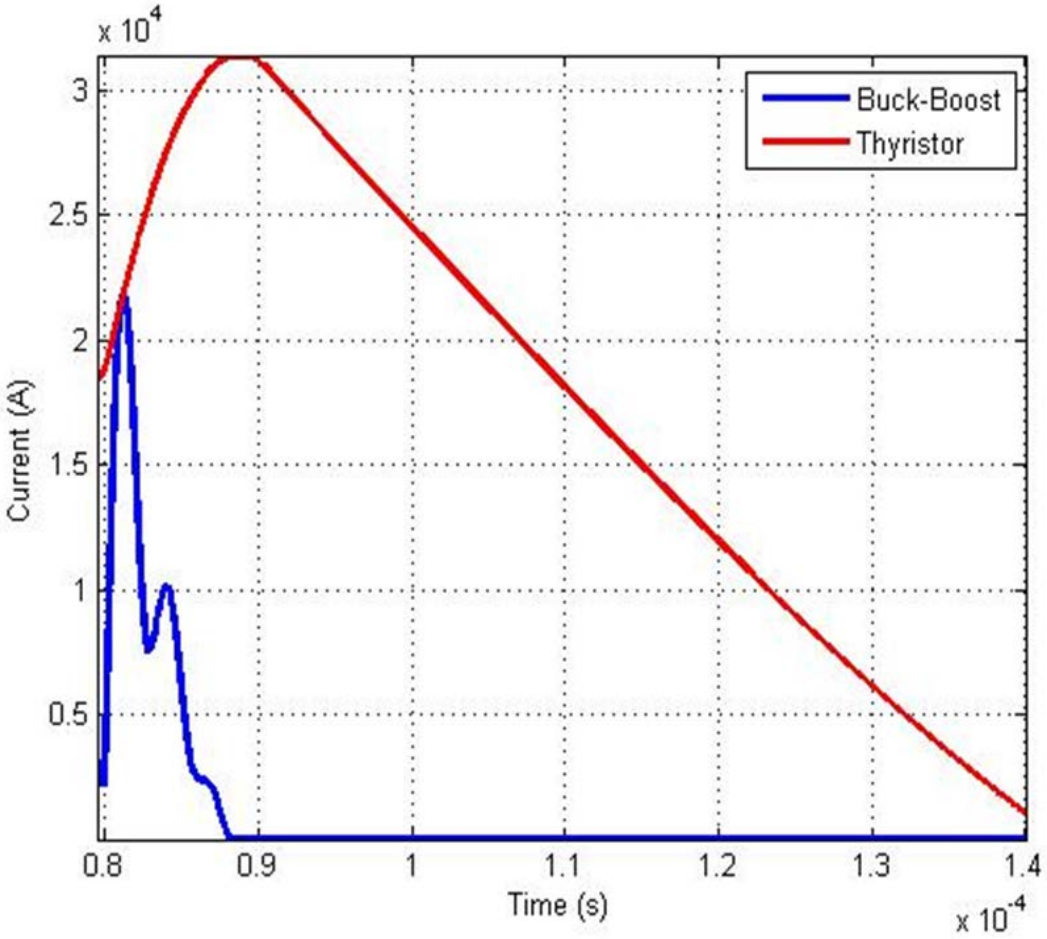

Figure 28. Buck-Boost Converter and Thyristor Post-Fire Arc Currents.

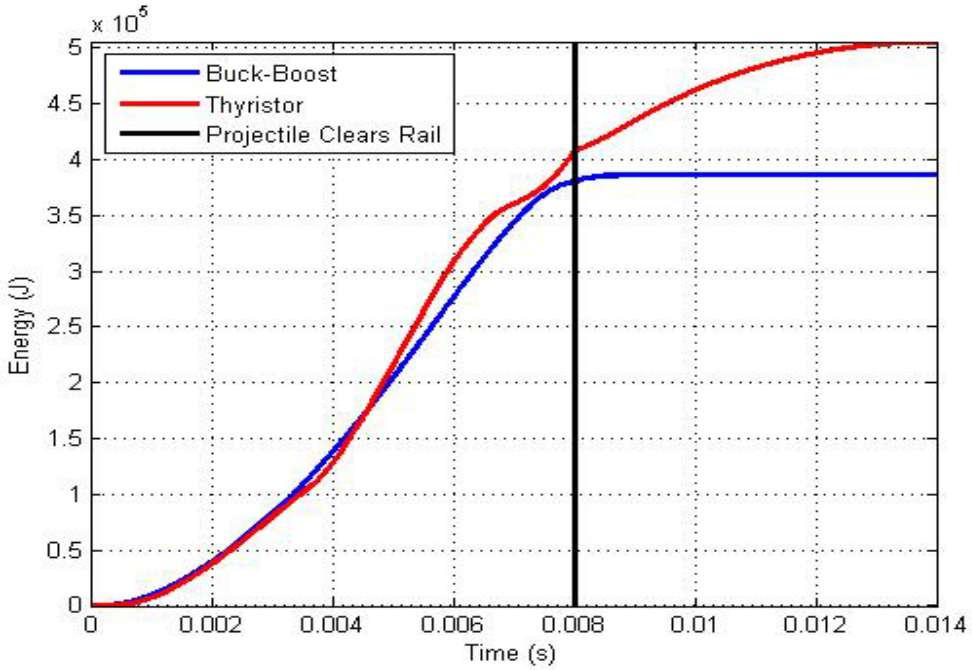

Figure 29. Buck-Boost Converter and the Thyristor Post-Fire Arc Energy.

Post-fire arcing in the rail delivered by the buck-boost converter circuit is comparatively less than that of the thyristor circuit. The buck-boost converter circuit delivered 114.0 A of calculated arc current after the armature exits the rail, this equates to 390.6 J of arc energy. When compared to the thyristor circuit, 79.4 kJ of arc energy is delivered to the rail over a 6.0-ms period. The arcing characteristic of both circuits for the same initial input capacitor energy are shown in Table 4.

Table 4. Arc Calculation for Buck-Boost and Thyristor Circuits.

Variable	**Buck-Boost**	**Thyristor**	**Ratio**
Arc Energy	390.597 J	79.454 kJ	0.005
Rail Energy	0.393 MJ	0.367 MJ	0.93
Capacitor Energy	0.441 MJ	0.441 MJ	1

The current delivered to the rails and the resulting energy delivered by the buck-boost converter and the thyristor circuit differ in many areas. The buck-boost rail current is relatively linear for the duration of time the projectile is in the rails. Comparatively, the thyristor rail current is characterized by the behavior of the input capacitor. When the thyristor is gated on, it remains on until the input capacitor is fully discharged. The characteristic of the current delivered to the rails by the thyristor circuit is due to the commutation of each capacitor within the circuits. A plot of the rail current as a function of both circuits is shown in Figure 30.

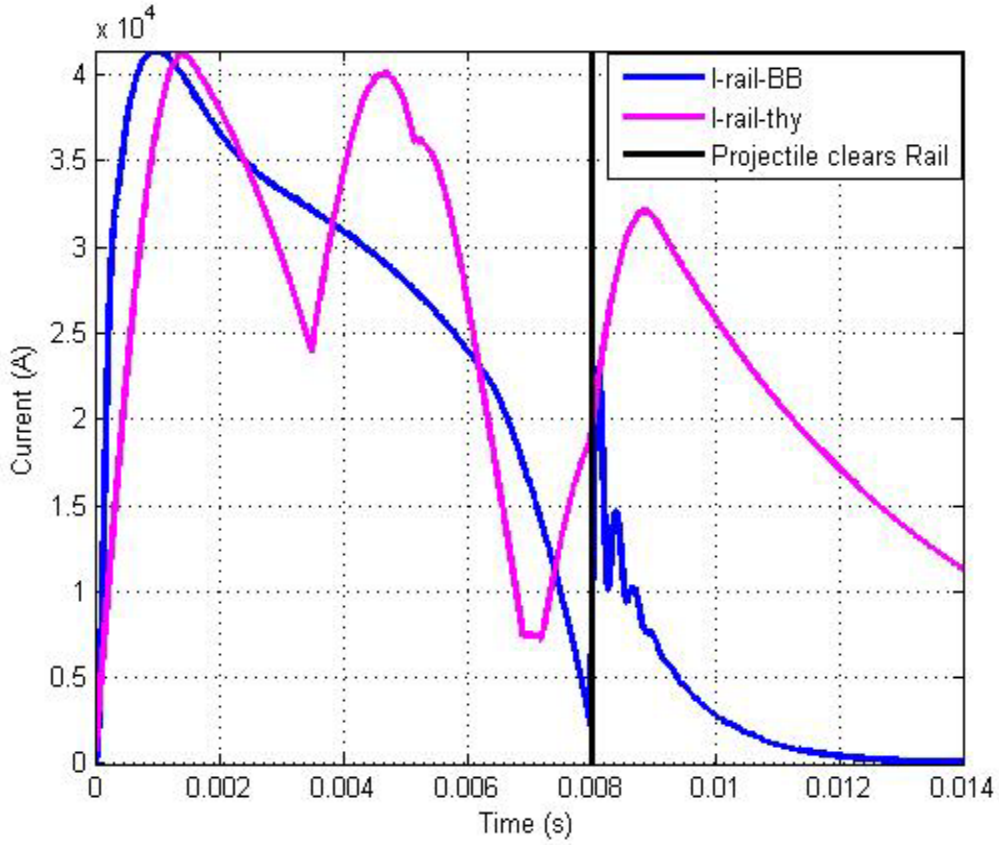

Figure 30. Buck-Boost Converter and Thyristor Rail Current.

After the projectile exits the rails, the amount of current that resides in the rails is the area where the buck-boost converter shows promises over the thyristor circuit. As shown in Figure 31, the current delivered to the rails by the thyristor circuit after the armature exits remains relatively high. In contrast to the thyristor circuit, after the armature exits the rails, the current delivered to the rails from the buck-boost converter immediately dissipates to zero within 6.0 ms. Given the same initial input capacitor energy of 0.441 MJ, the buck-boost converter delivered 0.380 MJ of energy to the rails. From the total rail energy delivered by the buck-boost circuit, 5.50 kJ of energy is dissipated in the rail after the projectile exits. This is 0.1205 MJ less than the thyristor circuit, which delivered 0.126 MJ of energy to the rails. The total energy delivered to the rails by the buck-boost converter circuit and the thyristor circuit is shown in Figure 32. Table 5 outlines the energy differences between the buck-boost converter circuit and the thyristor circuit.

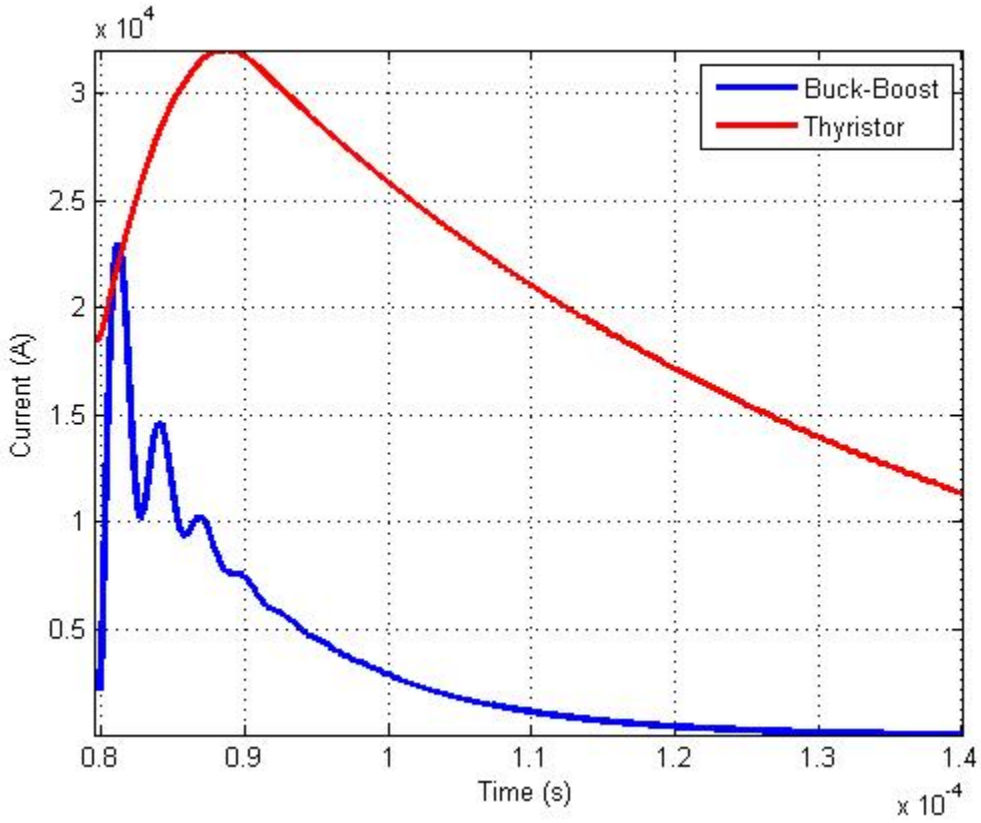

Figure 31. Post-Fire Rail Current for Both Buck-Boost Converter and Thyristor Circuit for a Resistor.

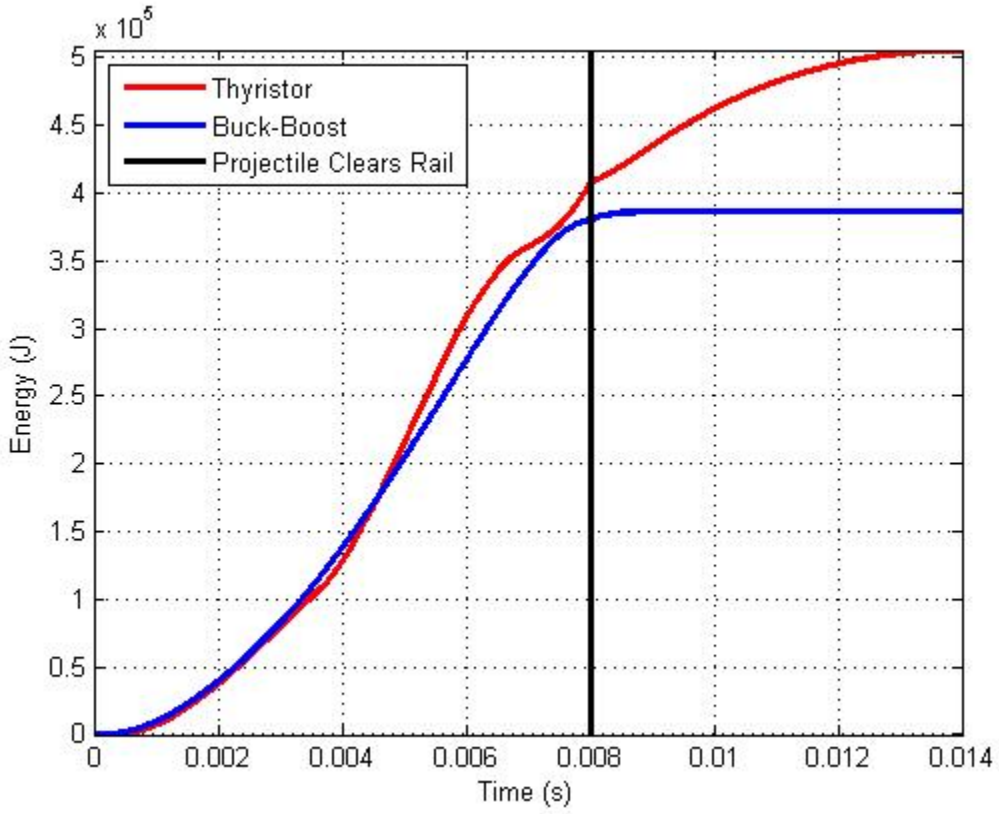

Figure 32. Total Energy Delivered to the Railgun by the Buck-Boost Converter Circuit and the Thyristor Circuit.

Table 5. Energy Calculation for the Buck-Boost Converter and Thyristor Circuit.

Variable	**Buck-Boost**	**Thyristor**	**Ratio**
Post-Fire Energy	5.50 kJ	0.126 MJ	0.043
Total Rail Energy	0.380 MJ	0.407 MJ	0.934
Capacitor Energy	0.441 MJ	0.441 MJ	1
Remaining Capacitor Energy	61 kJ	34 kJ	0.56

In summary, our analysis of the post-fire energy in the rails revealed that for the same initial input energy, the thyristor and buck-boost converter delivered approximately the same amount of energy to the rails. The buck-boost converter circuit showed enormous advantages over the thyristor circuit in our post-fire analysis. Based on data for the muzzle arc and the post-fire energy in a resistor for both railgun pulse-forming networks, the buck-boost converter is the preferred power supply architecture because it minimizes the muzzle flash and the associated thermal damages to the railgun.

THIS PAGE INTENTIONALLY LEFT BLANK

V. CONCLUSION

A. ACCOMPLISHMENTS

The framework of this thesis was to compare two railgun pulse-power supplies by quantifying their associated post-fire energy using Simulink. Using Simulink, we constructed an equivalent model for the buck-boost and the thyristor circuits. In addition to the circuit models, we constructed an equivalent railgun model, which was necessary to illustrate some characteristics of both circuits. The circuits' characteristics analyzed in this thesis included circuit current characteristics, energy to the rails, armature velocity, post-fire arcing and post-fire energy into a resistor. Appendix A shows the full Simulink model of this thesis and appendix B is the Matlab code used to generate plots.

Our analysis of the railgun as a function of the currents delivered by both circuits revealed that the buck-boost converter and thyristor circuit transferred energy to the rails with the same level of efficiency. The armature velocity and calculated kinetic energy plots for both circuits showed relative similarities. From simulated data, we concluded that the buck-boost converter could replace the current railgun power supply topology. Both circuits delivered similar current levels to the rails given the same initial input energy. The area where the buck-boost converter shows promise over the thyristor was in post-fire analysis.

Analysis of the railgun post-fire energy and post-fire arc demonstrated that the thyristor railgun power supply delivers 0.1205 MJ more than the proposed buck-boost power supply architecture to the rail in the form of an arc after the armature had exited the rails. This is because the current thyristor power supply delivers more current to the rails than the buck-boost converter circuit after the projectile has exited the rails. This continued supply of current was discharged into the rails at the muzzle, producing high temperature arcs. Contrary to the thyristor power supply, the buck-boost converter topology allows control of the rail current. In so doing, current delivery to the rails can be stopped when the armature exits the rails. This minimizes the discharge of high-energy arcs at the muzzle, thereby diminishing thermal damage to the rails.

B. FUTURE WORK

Additional research on the buck-boost converter circuit is necessary to determine its viability as an appropriate power supply topology for the railgun. The results of the simulation reported in this thesis support the theory that the buck-boost topology is superior to the thyristor topology in minimizing post-fire energy. To further support this theory, laboratory experimentation of the buck-boost circuit is imperative. A buck-boost PFN could be built and analyzed to acquire experimental data on the system characteristics and the post-fire energy.

APPENDIX A. SIMULINK MODEL

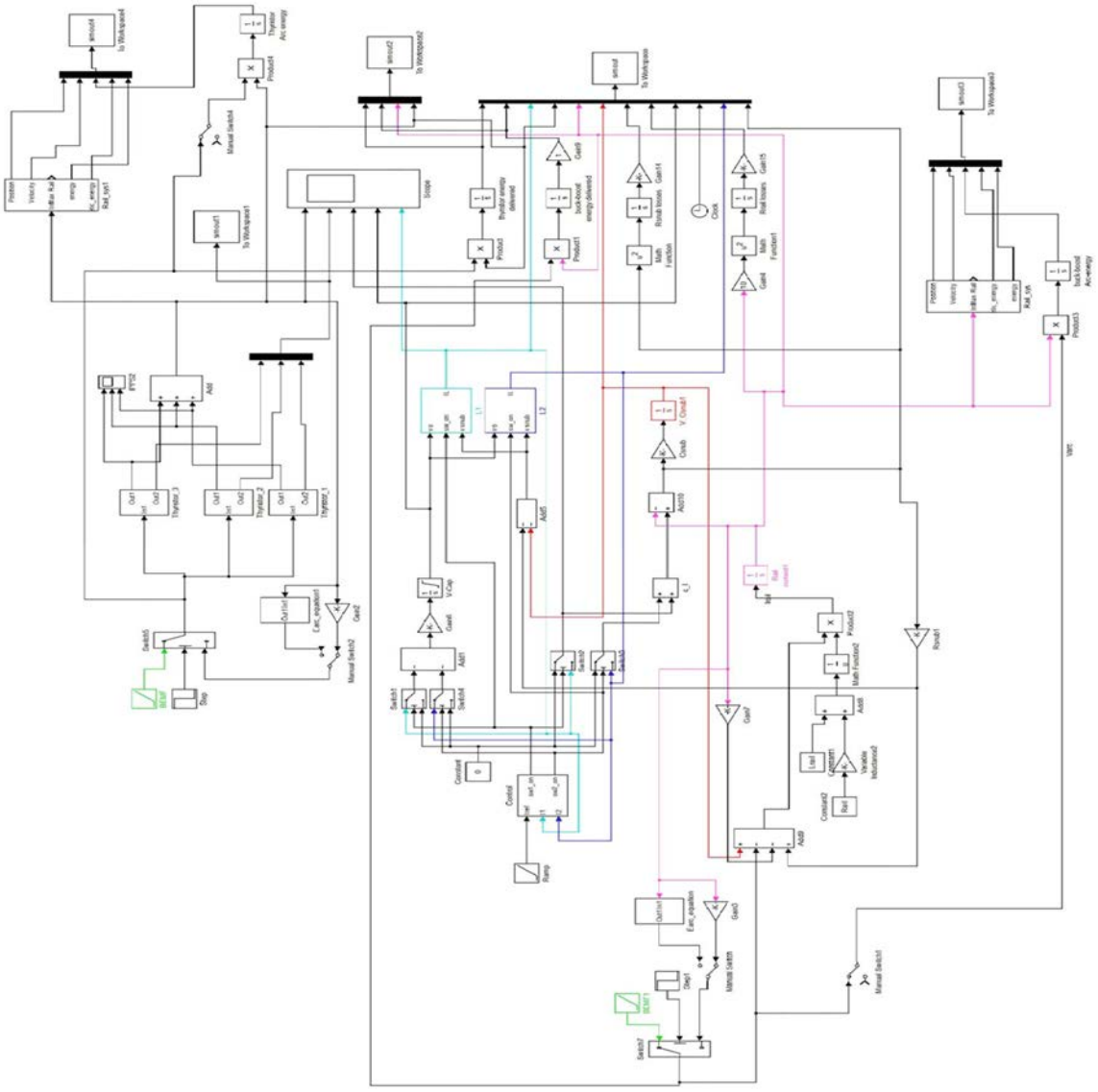

Figure 33. Simulink Model of Railgun Systems.

THIS PAGE INTENTIONALLY LEFT BLANK

APPENDIX B. MATLAB FILES

A. MATLAB INITIAL CONDITION FILES

```
tstep=4e-8;
vic=7000; %Source Capacitor starting voltage
vbemf=5000/.01;
C=6e-3; %Source Capacitance
Csnub=30e-5; %Rail Snubber capacitance
Rsnub=.05; %Rail Snubber resistance
Lrail=20e-6; %Rail initial inductance
Lprime=5e-7; %Rail variable inductance
Rprime=6e-5; %Rail variable resistance
R20=6e-5;%Rail and cable initial resistance
L=150e-6;
Rrail=0.001;
Kp=0.00004;
Ki=0.06;
Parc = 0.030;

m=3.125; %armature mass (kg)
Rail=8; %Rail length (m)
Railspace=500; %Rail separation (mm)
minCV=200; %minimum source capacitor voltage
IPPS=2e6; %Target constant current for rail
Isup=IPPS/Supplies; %Target current per supply
Imod=Isup/Modules; %Target current per module

Lpwm=20e-6; %Power supply inductance
fmod=1e5; %Power supply switching frequency
R_L=0.001; %Buck-Boost Inductor Resistance
Vdiode=5; %Blocking diode forward voltage drop
Rdiode=0.002/100; %Blocking diode forward resistance
Rsat=0.1/100; %IGBT forward resistance
Vcesat=7; %Voltage drop across saturated IGBT
Vbreakdown=15000; %Breakdown voltage of switches and diodes
BreakdownV=32.572; %Breakdown voltage factor
Ibreakdown=1e-200; %Breakdown reverse current for diode
Vth=0.026; %Thermal voltage of diode
Ileak=1500/(exp((6-1500*Rdiode)/Vth)-1); %Diode reverse bias leakage
current
DioderesistanceshiftV=2.85; %Voltage where diode shifts from
exponential to linear
DioderesistanceshiftI=Ileak.*(exp(DioderesistanceshiftV/Vth)-1);
%Current where diode shifts from exponential to linear
CDiode=1e-8; %Capacitance of diodes
```

B. MATLAB PLOT FILE

```
E_thy=simout(:,1);
v_length=length(E_thy);
E_buck_boost=simout(:,2);
I_buck_boost_L=simout(:,3);
I_thy=simout(:,4);
I_Lrail=simout(:,5);
V_Csnub=simout(:,6);
E_Rsnub=simout(:,7);
E_Rrail=simout(:,8);
V_Cap=simout(:,9);
time=simout(:,10);
I_buck_boost_L2=simout(:,11);
I_Lrail_thy=simout1(:,1);
BB_current = simout2.signals.values(:,3);
E_arc_BB = simout3(:,3);
BB_displacement = simout3(:,1);
BB_velocity = simout3(:,2);
BB_K_energy = simout3(:,4);
BB_Rail_E = simout3(:,5);
Thy_displacement = simout4(:,1);
Thy_velocity = simout4(:,2);
E_arc_Thy = simout4(:,3);
Thy_K_energy = simout4(:,4);
Rail_E_Thy = simout4(:,5);


%% Railgun Efficiency Estimate%%

% Wn    %Energy removed from the PFN
%%.....................................

% I_thyristor1 = simout1(:,1);
V_thyristor1 = simout1(:,1);

Load_E_thyristors = simout2.signals.values(:,1);
Load_E_buck_boost = simout2.signals.values(:,2);
time2 = simout2.time(:,1);

Load_I_BB = simout2.signals.values(:,3);
Load_I_thy = simout2.signals.values(:,4);

post_fire_E_Thy = Load_E_thyristors(198752:350001);
post_fire_E_BB = Load_E_buck_boost(198752:350001);

timex = time(198752:350001);

% PF_Energy_thy = trapz(timex,post_fire_E_Thy)/0.06;
% PF_Energy_BB = trapz(timex,post_fire_E_BB)/0.06;

post_fire_I_Thy = Load_I_thy(198752:350001);
```

```
post_fire_I_BB = Load_I_BB(198752:350001);

PF_I_thy = trapz(timex,post_fire_I_Thy)/0.06;
PF_I_BB = trapz(timex,post_fire_I_BB)/0.06;

PF_Energy_thy = (Parc*PF_I_thy*PF_I_thy);
PF_Energy_BB = (Parc*PF_I_BB*PF_I_BB);

timey = time(1:198751);

Arm_E_BB = trapz(timey,BB_K_energy(1:198751)/0.008);
Arm_E_thy = trapz(timey,Thy_K_energy(1:198751)/0.008);

E_BB = trapz(timey,BB_Rail_E(1:198751))/0.08;
E_Thy = trapz(timey,Rail_E_Thy(1:198751)/0.08);

total_BB_Irail = trapz(timey,I_Lrail(1:198751)/0.08);
total_thy_Irail = trapz(timey,I_thy(1:198751)/0.08);

KE_BB = trapz(timey,BB_K_energy(1:198751)/0.08);
KE_Thy = trapz(timey,Thy_K_energy(1:198751)/0.08);

I_Csnub=simout(:,12);
E_initial_thy=1/2*C*vic^2;
E_initial_buck_boost=3*1/2*C*vic^2;
E_Rrail_thy=sum(Rrail*I_thy.*I_thy)*tstep;
E_Rrail_BB =sum(Rrail*I_Lrail.*I_Lrail)*tstep;
E_balance_thy=E_initial_thy-E_thy(v_length)-E_Rrail_thy
E_balance_buck_boost=E_initial_buck_boost...
  -E_buck_boost(v_length)...
  -1/2*Csnub*V_Csnub(v_length)^2 ...
  -1/2*Lrail*I_Lrail(v_length)^2 ...
  -1/2*Lpwm*I_buck_boost_L(v_length)^2 ...
  -1/2*Lpwm*I_buck_boost_L2(v_length)^2 ...
  -E_Rsnub(v_length)...
  -E_Rrail(v_length)...
  -1/2*C*3*V_Cap(v_length)^2

ratio=E_buck_boost(v_length)/3/E_thy(v_length)

figure(1)
plot(time,E_buck_boost,'r','LineWidth',2)
hold on;
plot([0.008,0.008],[0,max(E_buck_boost)],'k','LineWidth',2)
% annotation('textarrow',[.3 .5],[.6 .5],'string', 'Post Fire Energy')
% annotation('textarrow',[.3 .5],[.6 .5],'string', 'BB-PFE = 2.916e4
J')
% annotation('textarrow',[.3 .5],[.6 .5],'string', 'Thy-PFE = 3.597e4
J')
legend('BB Rail Energy','Projectile clears
Rail','Location','northWest');
axis tight; xlabel('Time (seconds)'); ylabel('Energy (joules))');
% title('Rail Energy form BB-converter and Thyristors');
```

```
grid on;

% hold on; time,E_thy,'b',
% plot([0.008,0.008],[0,494692.541420790],'k','LineWidth',3)
% ,'Projectile clears Rales'

figure(2)
plot(time,I_Lrail,time,I_thy,'m','LineWidth',2)
hold on;
plot([0.008,0.008],[0,max(I_thy)],'k','LineWidth',2)
legend('I-rail-BB','I-rail-thy','Projectile clears
Rail','Location','southwest');
axis tight; xlabel('Time (seconds)'); ylabel('Current (amperes)');
% title('Positive Buck-Boost Converter & Thyristor Rail currents vs.
Time');
grid on;

% figure(2)
% plot(time,I_thy,'b','LineWidth',2)
% hold on;
% plot([0.008,0.008],[0,max(I_thy)],'k','LineWidth',2)
% legend('I-rail-thy','Projectile clears Rail','Location','southwest');
% axis tight; xlabel('Time (seconds)'); ylabel('Current (amperes)');
% % title('Positive Buck-Boost Converter & Thyristor Rail currents vs.
Time');
% grid on;

figure(3)
plot(time,I_thy,'b',time,I_buck_boost_L2*1.5,'r','LineWidth',2)
hold on;
plot([0.008,0.008],[0,max(I_thy)],'k','LineWidth',2)
legend('Thy-current','BB-current');
axis tight; xlabel('Time (seconds)'); ylabel('Current (amperes)');
title('Positive Buck-Boost Converter & Thyristor current vs. Time');
grid on;

% figure(3)
% plot(time,I_buck_boost_L2*1.5,'r','LineWidth',2)
% % legend('Thy-current');
% axis tight; xlabel('Time (seconds)'); ylabel('Current (amperes)');
% % title('Positive Buck-Boost Converter & Thyristor current vs.
Time');
% grid on;

figure(4)
plot(time,V_Csnub)
axis tight; xlabel('Time (seconds)'); ylabel('Voltage
(voltages)','LineWidth',2);
title('Snubber Voltage vs. Time');
grid on;

figure(5)
plot(time,I_buck_boost_L,time,I_buck_boost_L2,time,I_Csnub,time,-
I_Lrail,'LineWidth',2)
```

```
legend('I_1','I_2','I_C','-I_r_a_i_l','North');
grid on;

figure(6)
plot(time,I_buck_boost_L,'r',time,I_buck_boost_L2,'LineWidth',2)
legend('I-buck-boost-L','I-buck-boost_L2','North');
axis tight; xlabel('Time (seconds)'); ylabel('Current (amperes)');
title('Positive Buck-Boost Converter current vs. Time');
grid on;

figure(7)
plot(time2,Load_E_thyristors,'r',time2,Load_E_buck_boost,'b','LineWidth
',2)
hold on;
plot([0.008,0.008],[0,max(Load_E_thyristors)],'k','LineWidth',2)
legend('Thyristor','Buck-Boost','Projectile Clears
Rail','Location','northwest')
axis tight; xlabel('Time (seconds)'); ylabel('Energy (joules)');
% title('Thyristor and Buck-Boost Rail Energy vs. Time');
grid on;

timeyx = time(198752:350001);

% figure(7)
plot(timeyx,post_fire_E_BB,'b',timeyx,post_fire_E_Thy,'r','LineWidth',2
)
% legend('Buck-Boost','Thyristor','Location','northeast')
% axis tight; xlabel('Time (seconds)'); ylabel('Energy (joules)');
% title('Thyristor and Buck-Boost Rail Energy vs. Time');
% grid on;

figure(8)
plot(time,V_thyristor1,'r',time, V_Cap,'g','LineWidth',2)
hold on;
plot([0.008,0.008],[0,max(V_thyristor1)],'k','LineWidth',2)
legend('Thyristor','Buck-Boost','West')
axis tight; xlabel('Time (seconds)'); ylabel('Voltage (voltages)');
title('Buck-Boost and Thyristor Voltage vs. Time');
grid on;

figure(9)
plot(time,E_arc_BB,'b',time,E_arc_Thy,'r','LineWidth',2)
hold on;
plot([0.008,0.008],[0,max(E_arc_Thy)],'k','LineWidth',2)
legend('Buck-Boost','Thyristor','Projectile Clears
Rail','Location','northWest')
axis tight; xlabel('Time (seconds)'); ylabel('Energy (joules)');
% title('Buck-boost and Thyristor Arc');
grid on;

figure(10)
plot(time,E_Rrail)
axis tight; xlabel('Time (seconds)'); ylabel('Energy (joules)');
title('Rail Energy');
```

```
grid;

figure(11)
plot(time,BB_displacement,'b',time, Thy_displacement,'r','LineWidth',2)
legend('Buck-Boost','Thyristor','Location','northWest')
axis tight; xlabel('Time (seconds)'); ylabel('Distance (meters)');
% title('Buck-Boost and Thyristor Voltage vs. Time');
grid on;

figure(12)
plot(time,BB_velocity,'b',time,Thy_velocity,'r','LineWidth',2)
hold on;
plot([0.008,0.008],[0,max(Thy_velocity)],'k','LineWidth',2)
legend('Buck-Boost','Thyristor','Projectile Clears
Rail','Location','northWest')
axis tight; xlabel('Time (seconds)'); ylabel('Velocity (meters per
second)');
% title('Buck-Boost and Thyristor Voltage vs. Time');
grid on;

% figure(12)
% plot(time,Thy_velocity,'r','LineWidth',2)
% hold on;
% plot([0.008,0.008],[0,max(Thy_velocity)],'k','LineWidth',2)
% legend('Thyristor','Projectile Clears Rail','Location','northWest')
% axis tight; xlabel('Time (seconds)'); ylabel('Velocity (meters per
second)');
% % title('Buck-Boost and Thyristor Voltage vs. Time');
% grid on;

figure(13)
plot(time,Rail_E_Thy*0.08,'r',time, Thy_K_energy,'g','LineWidth',2)
hold on;
plot([0.008,0.008],[0,max(Thy_K_energy)],'k','LineWidth',2)
legend('Rail energy','Armature Energy','Projectile Clears
Rail','Location','northWest')
axis tight; xlabel('Time (seconds)'); ylabel('Energy (Joules)');
% title('Buck-Boost and Thyristor Voltage vs. Time');
grid on;

% figure(13)
% plot(time, Thy_K_energy,'g','LineWidth',2)
% legend('Rail energy','Armature Energy','Location','northWest')
% axis tight; xlabel('Time (seconds)'); ylabel('Energy (Joules)');
% % title('Buck-Boost and Thyristor Voltage vs. Time');
% grid on;

figure(14)
plot(time,BB_Rail_E*0.08,'r',time, BB_K_energy,'g','LineWidth',2)
hold on;
plot([0.008,0.008],[0,max(BB_Rail_E*0.08)],'k','LineWidth',2)
legend('Rail energy','Armature Energy','Projectile Clears
Rail','Location','northWest')
axis tight; xlabel('Time (seconds)'); ylabel('Energy (Joules)');
```

```
% title('Buck-Boost and Thyristor Voltage vs. Time');
grid on;

figure(15)
plot(time,BB_K_energy,'g',time, Thy_K_energy,'m','LineWidth',2)
hold on;
plot([0.008,0.008],[0,max(Thy_K_energy)],'k','LineWidth',2)
legend('Armature Energy BB','Armature Energy THY','Projectile Clears
Rail','Location','northWest')
axis tight; xlabel('Time (seconds)'); ylabel('Energy (joules)');
% title('Buck-Boost and Thyristor Voltage vs. Time');
grid on;

% planar EI
% E102

%Lpwm*1e3*400^2
AL=9997   % P type
LE=14.8   % cm
Lg=.2    % cm
ue=1/(1/2500+Lg/LE)
turns=sqrt(Lpwm/1e-6*1000/AL)
H=turns*400/LE/.8
```

THIS PAGE INTENTIONALLY LEFT BLANK

LIST OF REFERENCES

[1] Railgun theory. (n.d.). Wikipedia. [Online]. Available: https://en.wikipedia.org/wiki/Railgun. Accessed Dec 10. 2015

[2] A. L. Julian, J. H. Black and W. B. Maier II, "Power supply design for high voltage capacitor discharge railgun supply using thyristors," in *Electromagnetic Launch Technology, 2008 14th Symposium on,* 2008, pp. 1–5.

[3] M. J. Fisher, *Power Electronics*, 1st ed. Boston, MA: PWS-KENT, 1991, pp. 36–81.

[4] Railgun schematic. 3dprint. (n.d.). [Online]. Available: https://3dprint.com/101512/3d-printed-working-railgun/. Accessed Apr 21. 2016

[5] B. Maier, "Selected topics in railgun technology," class notes for Railgun Physics, Dept. of Phys., Naval Postgraguate School, Monterey, CA, Spring 2012.

[6] R. F. Ammerman, T. Gammon, P. K. Sen and J. P. Nelson, "Dc arc models and incident energy calculations," In *Industry Applications Society 56th Annual Petroleum and Chemical Industry Conference,* 2009, pp. 1–13.

[7] A. Martino, "Theory and design of medium voltage pulsed current supply using wide band gap solid state device," Ph.D. dissertation, Dept. Elect. Eng., Naval Postgraduate School, Monterey, CA, 2015.

[8] J. S. Bernardes, G. P. LaCava and M. J. Schrader, "Analysis of a railgun capacitor-muzzle-shunt energy recovery scheme," Power Modulator Symposium, *Conference Record of the Twenty-Fifth International High-Voltage Workshop,* 2002, pp. 347–350.

THIS PAGE INTENTIONALLY LEFT BLANK

INITIAL DISTRIBUTION LIST

1. Defense Technical Information Center
   Ft. Belvoir, Virginia

2. Dudley Knox Library
   Naval Postgraduate School
   Monterey, California